Radboud Repository

Radboud University Nijmegen

PDF hosted at the Radboud Repository of the Radboud University Nijmegen

The following full text is a publisher's version.

For additional information about this publication click this link.
http://hdl.handle.net/2066/114051

Please be advised that this information was generated on 2017-12-06 and may be subject to change.

3025

ELECTRON FOCUSING IN METALS

P. A. M. Benistant

ELECTRON FOCUSING IN METALS

P R O E F S C H R I F T

TER VERKRIJGING VAN DE GRAAD VAN DOCTOR IN DE
WISKUNDE EN NATUURWETENSCHAPPEN
AAN DE KATHOLIEKE UNIVERSITEIT TE NIJMEGEN, OP GEZAG VAN
DE RECTOR MAGNIFICUS PROF. DR. J.H.G.I. GIESBERS,
VOLGENS BESLUIT VAN HET COLLEGE VAN DEKANEN
IN HET OPENBAAR TE VERDEDIGEN
OP WOENSDAG 3 OKTOBER 1984
DES NAMIDDAGS TE 4.00 UUR

door

PETRUS ALPHONSUS MARIA BENISTANT
geboren te Amsterdam

1984
Druk: Krips Repro Meppel

PROMOTOR
PROF. DR P WYDER

CO-REFERENT:
DR. H. VAN KEMPEN

Voor mijn ouders

Mieke

Esther

Op deze pagina wil ik iedereen bedanken die mij, direct of indirect, geholpen heeft met het tot stand komen van dit proefschrift. In het bijzonder Riki Gommers en de technici Kees Beers, Jan Hermsen en Jan Gerritsen voor hun nimmer aflatende hulpvaardigheid en Peter Schroeder voor zijn waardevolle opmerkingen. Verder alle medewerkers van de afdeling Experimentele Natuurkunde 4 voor de prettige samenwerking in de afgelopen vier jaar. Niet in de laatste plaats, Mieke en Esther voor hun morele steun.

Dit onderzoek werd verricht op de afdeling Experimentele Natuurkunde 4 van het Research Instituut voor Materialen van de Katholieke Universiteit te Nijmegen, onder leiding van Prof. Dr. P. Wyder. Een gedeelte van dit onderzoek werd gesteund door de Stichting voor Fundamenteel Onderzoek der Materie (FOM) met financiële bijdragen van de Nederlandse Organisatie voor Zuiver Wetenschappelijk Onderzoek (ZWO).

CONTENTS

One of the most striking properties of metals in contrast to other solids is their high electrical conductivity. In metals a group of electrons, the so called conduction electrons, can respond to an electric field and produce an electric current. Three years after J. J. Thomson in 1897 had discovered the electron, P. Drude[1] constructed his theory of electrical and thermal conduction, by considering a metal as a gas of electrons and applying the kinetic theory of gases to it. Drude assumed that the electrons moved freely through the metal, being scattered by the metal ions only (Fig. 1.1). The electrons achieved thermal

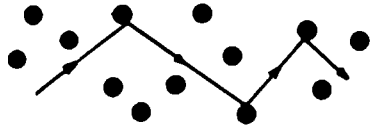

Fig. 1.1
Trajectory of a conduction electron scattering off the ions, according to Drude's theory.

equilibrium with their surroundings only through these collisions. Shortly after the discovery that the Pauli exclusion principle was needed to account for the bound electronic states of atoms, Sommerfeld[2] applied the same principle to the free electron gas of metals. In Sommerfeld's model the electron levels are quantized and therefore the electronic energy distribution is taken to be the quantum Fermi-Dirac distribution rather than the classical Maxwell-Boltzmann distribution (Fig. 1.2). As a consequence the electrons in a metal occupy energy levels up to a particular energy (at zero temperature), the Fermi energy. The surface in wave vector space, which separates occupied from unoccupied electron levels, is called the Fermi surface. In the free electron model it is a sphere.

The free electron model does not take into account the fact that the metal ions are not distributed at random, but are arranged in a regular periodic array, the crystal lattice. This was first directly confirmed by X-ray diffraction experiments and subsequently reconfirmed by neutron diffraction, electron microscopy, and many other direct measurements.

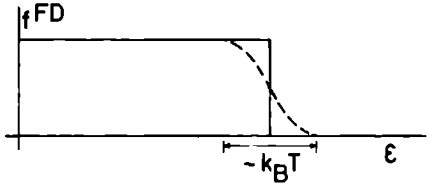

Fig. 1.2
The Fermi-Dirac distribution. At $T = 0$ all electron levels up to the Fermi energy ε_F are occupied, while at finite temperatures some electrons just below ε_F have been excited to levels just above ε_F.

The lattice structure of the metal, in real space, and the number of conduction electrons per atom largely determine the shape of the Fermi surface in wave vector ($\vec{k}$) space. Because it is intimately involved in the transport coefficients as well as in the equilibrium and optical properties of the metal, the importance of determining the Fermi surface of metals is clear.

Of the many techniques, which have been used already to deduce the geometry of the Fermi surface, the de Haas-van Alphen effect is one of the most powerful. In 1930 W. J. de Haas and P. M. van Alphen[3] measured the magnetization M of a bismuth sample as a function of magnetic field H in high fields at 14.2 K, and found oscillations in M/H. The full extent of its usefulness was pointed out in 1952 by Onsager[4], while the refinement of the de Haas-van Alphen effect into a powerful probe of the Fermi surface has been due largely to Shoenberg[5].

Other methods to examine Fermi surface properties are, for example, the Anomalous Skin Effect[6], where the reflection and absorption of microwave electromagnetic radiation is measured in pure metal single crystals with an electron mean free path greater than the skin depth; Cyclotron Resonance[7], where the frequency is measured at which an electric field resonates with the electronic motion in a uniform magnetic field; and the Gantmakher Effect[8], where again by using microwave radiation, extremal electron orbit diameters (or an integral multiple of them) are measured by placing a thin metal slab in a uniform magnetic field.

In 1965 Yu. V. Sharvin[9] introduced a new method for studying Fermi surfaces. He placed two point contacts on the opposite sides of a thin metal single crystal slab and focused electrons injected into the slab at one point contact, on to the other contact by means of a longitudinal

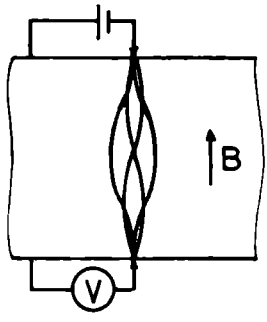

Fig. 1.3
Experimental arrangement of Sharvin. By a uniform magnetic field oriented perpendicular to the surface of the slab, electrons injected at one point contact, are focused on the opposite contact.

magnetic field (Fig. 1.3). In 1974 V. S. Tsoi[10] improved this method by placing the point contacts on the same side of the metal surface, and applying a transverse magnetic field, i.e. parallel to the metal surface but perpendicular to the line connecting the point contacts (Fig. 1.4). There are many advantages with this method:

1. Extremal diameters of discrete orbits on the Fermi surface are measured; the direction of the axis normal to the (real space) crystal surface determines the (wave vector space) direction in which these diameters are measured, the direction of the applied magnetic field determines the section in which the orbit lies on the Fermi surface.
2. If the direction of the applied magnetic field is not perpendicular to the line connecting the point contacts, however, extremal diameters of non-extremal orbits on the Fermi surface can be measured.
3. The extremal diameters are measured in small volumes under the crystal surface ($\sim$0.1 mm^3).
4. Specular reflection of electrons from the crystal surface can be observed, i.e. observation of the metal surface on an atomic scale "from within".
5. The scattering of electrons from other boundaries can be observed, e.g. crystallites and interfaces between metals or between a normal metal and a superconductor.

In this thesis is described a series of experiments, which applies the Tsoi method to study the focusing of electrons on different orbits of Fermi surfaces, and the interaction of electrons both with metal surfaces and with normal-metal-superconductor interfaces.

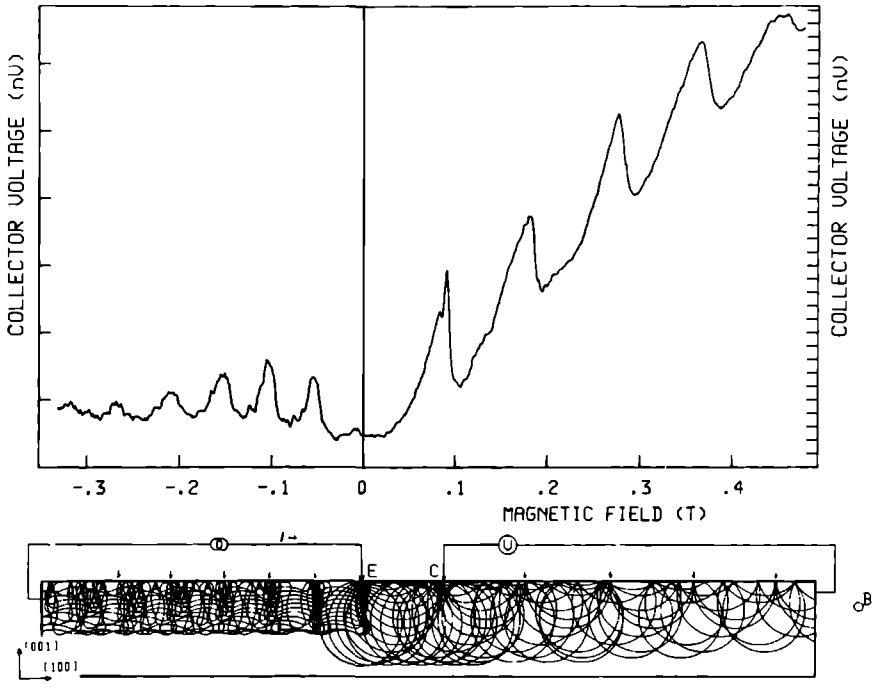

Fig. 1.4 Electron focusing in a metal single crystal. The lowest part of the figure shows the experimental arrangement as introduced by Tsoi. Electrons are injected into the crystal at E, and at C the voltage is measured as a function of applied magnetic field B. Electron paths in the crystal due to a uniform magnetic field have been plotted for electron- and hole-like orbits on the Ag Fermi surface. Arrows show the places where electron focusing takes place (directly and after specular reflections) at the crystal surface. The upper part of the figure shows the measured collector voltage as a function of applied magnetic field B, obtained from an Ag single crystal. Clearly the voltage peaks due to electron focusing can be seen. Because the magnetic field strength is inversely proportional to the radius of the electron orbits, the voltage peaks, measured at C, as a function of B coincide with the places where focusing takes place at the crystal surface in the lowest part of the figure. The different orbit types are identified by the different magnetic field orientations and strengths where the voltage peaks show up, and the different signal forms.

The thesis is organized as follows. In the next chapter a review is given of the experimental technique together with the theoretical background based on semiclassical theory, which is adequate for this technique. Experimental results from a pure silver single crystal are given and compared to calculated results.

The third chapter is an application of this technique to an aluminium single crystal. It is shown that the shape of the Fermi surface determines the magnetic field dependence of the collector voltage as well as the strength of the focusing field.

The last two chapters deal with the peculiar way an electron in a normal metal reflects from a normal-metal-superconductor interface, the so called Andreev reflection[11]. In the superconductor there exists a zone of forbidden energies, the energy gap, and an electron in the normal metal with an energy within this energy gap cannot flow into the superconductor. The electron cannot be reflected as an electron either, because there is no potential barrier at the interface. Instead, the electron is reflected as a hole in the normal metal, while simultaneously an electron pair is added to the condensate in the superconductor. With the use of the double point contact technique as well as the single point contact technique[12] the Andreev-reflected holes are focused, giving detailed information about the quality of the normal-metal-superconductor interface, but perhaps also about weak interactions of electrons and holes in the normal metal itself.

All chapters are given in the form of published papers or papers to be published.

References

1. P. Drude, Annalen der Physik 1, 556 and 3, 369 (1900).
2. A. Sommerfeld, Zeits. f. Physik 47, 1 (1928).
3. W. J. de Haas, and P. M. van Alphen, Leiden Comm. 208d, 212a (1930), and 220d (1932).
4. L. Onsager, Phil. Mag. 43, 1006 (1952).
5. D. Shoenberg, Prog. Low Temp. Phys. 2, 226 (1957).
6. A. B. Pippard, Phil. Trans. Roy. Soc. A250, 325 (1957).
7. M. I. Azbel', and E. A. Kaner, [Sov. Phys. -JETP 3, 772 (1956)].
8. V. F. Gantmakher, [Sov. Phys. -JETP 15, 982 (1962)].
9. Yu. V. Sharvin, Zh. Eksp. Teor. Fiz. 48, 984 (1965) [Sov. Phys. -JETP 21, 655 (1965)].
10. V. S. Tsoi, ZhETF Pis. Red. 19, 114 (1974) [JETP Lett. 19, 70 (1974)].
11. A. F. Andreev, Zh. Eksp. Teor. Fiz. 46, 1823 (1964) [Sov. Phys. -JETP 19, 1228 (1964)].
12. A. G. M. Jansen, A. P. van Gelder, and P. Wyder, J. Phys. C: Solid St. Phys. 13, 6073 (1980).

II ELECTRON FOCUSING IN SILVER

ABSTRACT

In this chapter we discuss the principles of magnetic focusing of electrons in a metal single crystal by means of point contacts. Both the shape and the amplitude of the measured signal are calculated as a function of applied magnetic field in the free electron approximation. Experimental results are given for two silver single crystals with a (001) and a (011) surface respectively. Different orbits on the Ag Fermi surface were observed, both extremal and non-extremal ones. The Fermi momenta obtained from these measurements agree with calculated ones. Also focusing is observed of electrons reflected specularly from the crystal surface. The coefficient for specular reflection was estimated to be 0.8 ± 0.1 for the (001) sample along the <100> directions and also for the (011) sample along the <100> and <111> directions.

2.1 *Introduction*

In 1965 Yu. V. Sharvin[1] introduced and realized[2,3] a new method for studying Fermi surfaces. Electrons injected into a thin metal single crystal through a point contact, were focused on another point contact, placed on the opposite side of the crystal, by means of a magnetic field

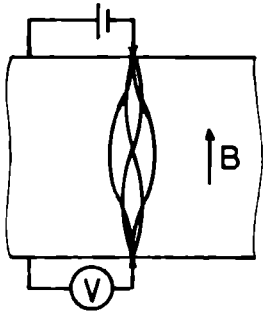

Fig. 2.1
Experimental arrangement of Sharvin. By a uniform magnetic field oriented perpendicular to the surface of the slab, electrons injected at one point contact, are focused on the opposite contact.

directed along the point contacts (Fig. 2.1). Because of the direction of the magnetic field this was called longitudinal electron focusing (LEF). Although the method worked in principle, experimentally it was very hard to get the two point contacts exactly opposite to each other on a metal slab of half a millimeter thickness. Therefore, in 1974, V. S. Tsoi[4] placed the point contacts on the same side of the crystal surface with the magnetic field directed parallel to the surface and perpendicular to the imaginary line connecting the point contacts (Fig. 2.2). Because now the magnetic field was directed perpendicular to the point contacts, this kind of focusing was called transverse electron focusing (TEF). The experimental technique is the same as that of Sharvin: electrons are injected through one point contact, the emitter (E), into the metal single crystal, and at the other point contact, the collector (C), the voltage is measured as a function of the applied field. Due to this field the electrons are bent around and will be able to reach the crystal surface again, provided that the mean free path is long enough. Fig. 2.3 illustrates that the electrons that are injected into the crystal perpendicular to the surface, are focused on to the

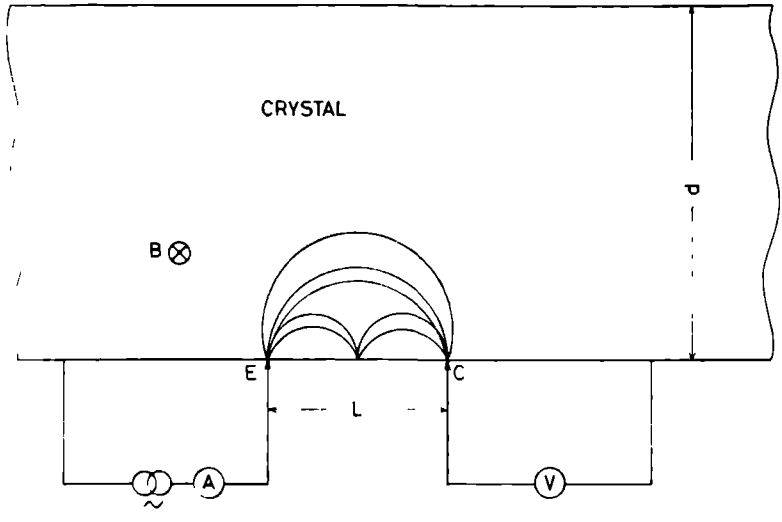

Fig. 2.2 Experimental arrangement of Tsoi. The two point contacts are placed on the same side of the crystal surface, and the magnetic field is oriented parallel to the surface and perpendicular to the line connecting the point contacts.

crystal surface. At a particular value of the applied field, B_0, the focusing will take place at the collector, giving rise to a voltage peak. Also at multiple field strengths, $B_1 = 2B_0$, $B_2 = 3B_0$, ..., voltage peaks can be measured due to electrons that have been reflected specularly from the crystal surface between the point contacts. Normally the electron orbits are not circular. As will be discussed below, in wave vector ($\vec{k}$) space the electrons move over orbits given by the intersection of surfaces of constant energy (e.g. the Fermi surface) with planes perpendicular to the applied magnetic field. The projection of the real space orbit in a plane perpendicular to the magnetic field is the same as the k-space orbit rotated through 90° about the field direction. Therefore, with this technique not only can extremal diameters of intersections of the Fermi surface be determined, but also the properties of the surface of the crystal itself as seen from the inside.

This technique has been employed succesfully on various metals and semi metals: bismuth[4,5], antimony[6], tungsten[7,8,9], copper[7,10,11], silver[12,13], aluminium[14].

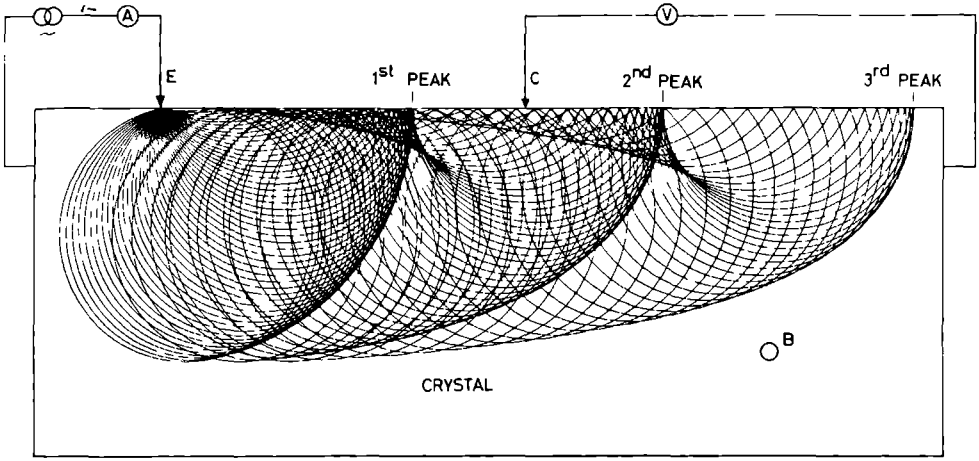

Fig. 2.3 Orbits of charged particles in a magnetic field, injected through a point contact (E); The electrons that are injected normally to the surface at E, are focused on to the crystal surface. Also focusing after specular reflection from the crystal surface can be seen.

2.2 *Electrons in a homogeneous magnetic field*

In this section expressions are derived for the strength of the applied magnetic field in the case of electron focusing, and the voltage across the collector contact as a function of the applied field. The calculations are made for a spherical Fermi surface (free electron approximation), which is in good agreement with the real Ag Fermi surface, except in the <111> directions where bulges in the Fermi surface occur (see section 2.4).

It will appear in the following sections that the measured focusing field strengths are indeed in good agreement with those calculated using the free electron model, but that the shape of the collector voltage as a function of applied magnetic field as well as the intensity of the focusing peak are very sensitive to the exact shape of the Fermi surface.

The semiclassical equations of motion for an electron with a velocity $\vec{v}(\vec{k})$ in a homogeneous magnetic field are given by

$$\vec{v}(\vec{k}) = \frac{1}{\hbar} \frac{\partial \varepsilon(\vec{k})}{\partial \vec{k}} \tag{2.1}$$

$$\hbar \dot{\vec{k}} = (-e)\ \vec{v}(\vec{k}) \times \vec{B} \tag{2.2}$$

It follows immediately from these equations that the component of $\vec{k}$ along the magnetic field and the energy $\varepsilon(\vec{k})$ are both constants of the motion. This means that the electrons will move along curves given by tne intersection of surfaces of constant energy with planes perpendicular to the magnetic field. As $\vec{v}(\vec{k})$ points in k-space from lower to higher energies, $\vec{v}(\vec{k})$ points outwards if the orbit encloses lower energy bands, and the orbit is traversed clockwise, looking along the direction of the applied field. Such orbits are called electron orbits, because free electrons in a magnetic field would describe a circle in the same direction. Orbits enclosing higher energy bands are traversed in the opposite direction and are therefore called hole orbits, despite the fact that negatively charged electrons traverse them.

The projection of the real space orbit in a plane perpendicular to the direction of the magnetic field, $\vec{r}_\perp = \vec{r} - \hat{B}(\hat{B}\cdot\vec{r})$, can be found by taking the vector product of both sides of Eq. (2.2) with a unit vector parallel to the field. This yields

$$\hat{B} \times \hbar \dot{\vec{k}} = -eB \left[\dot{\vec{r}} - \hat{B}(\hat{B}\cdot\dot{\vec{r}})\right] = -eB\dot{\vec{r}}_\perp \tag{2.3}$$

which integrates to

$$\vec{r}_\perp(t) - \vec{r}_\perp(0) = -\frac{\hbar}{eB} \hat{B} \times [\vec{k}(t) - \vec{k}(0)] \tag{2.4}$$

From Eq. (2.4) it can be seen that the projection of the real space or-

bit in a plane perpendicular to the direction of the magnetic field is simply the k-space orbit, rotated through 90° about the field direction

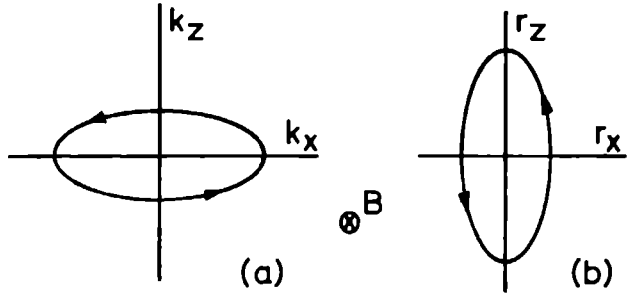

Fig. 2.4 Electron orbits in k-space (a) and real space (b) due to a uniform magnetic field.

and scaled by the factor $\hbar/eB$ (Fig. 2.4). The component of the real space orbit parallel to the field is given by

$$\vec{r}_{\parallel}(t) = \vec{r}_{\parallel}(0) + \int_0^t \vec{v}_{\parallel}(t')\,dt' \qquad \vec{v}_{\parallel} = \frac{1}{\hbar}\frac{\partial \varepsilon}{\partial \vec{k}_{\parallel}} \qquad (2.5)$$

In contrast to the free electron approximation, $\vec{v}_{\parallel}$ need not be constant, even though $\vec{k}_{\parallel}$ is. Therefore, the motion of the electron along the field need not be uniform.

2.2.2 *Electrons injected through a point contact*

If the electrons are injected into the crystal through a point contact (the emitter), $\vec{r}(0)$ is fixed. As both point contacts are placed on the same side of the crystal, we want to know where the electrons, describing closed orbits on the Fermi surface, arrive at the crystal surface again. Taking the surface in the xy-plane, the emitter at the origin, and the magnetic field directed along the y-axis, we have the following boundary conditions for electrons traversing closed orbits, that are symmetric with respect to the direction perpendicular to the

crystal surface (the z-axis)

$$\vec{r}(0) = (0,0,0) \qquad \vec{r}(T) = (r_x(T), r_y(T), 0) \tag{2.6}$$

$$\vec{k}(T) = (k_x(0), k_y(0), -k_z(0)) \tag{2.7}$$

with T the time an electron needs to arrive at the crystal surface again. Now Eq. (2.4) becomes

$$\vec{r}_{\perp}(T) = \hat{x}\, r_x(T) = -\frac{\hbar}{eB}\, \hat{B} \times \left[\vec{k}(T) - \vec{k}(0)\right] \tag{2.8}$$

or

$$r_x(T) = \frac{2\hbar}{eB}\, k_z(0) \tag{2.9}$$

This means that if, in the experiment, we keep the imaginary line connecting the point contacts perpendicular to the direction of the applied field, i.e., along the x-axis, we have only to deal with the component of the wave vector perpendicular to the crystal surface. For free electrons $\varepsilon = \hbar^2 k^2/2m$, yielding a spherical Fermi surface. Defining polar coordinates in such a way that ϕ is the angle of $\vec{k}(0)$ with the positive y-axis, and α the angle of the projection of $\vec{k}(0)$ on the xz-plane with the negative z-axis (Fig. 2.5), $\vec{k}(0)$ becomes

$$\vec{k}(0) = k_F(\sin\alpha\sin\phi, \cos\phi, -\cos\alpha\sin\phi) \qquad -\frac{\pi}{2} < \alpha < \frac{\pi}{2},\ 0 < \phi < \pi \tag{2.10}$$

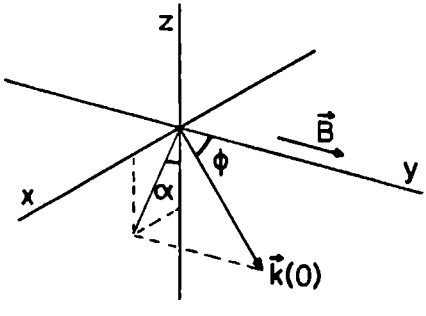

Fig. 2.5
Definition of α and ϕ. The upper crystal surface lies in th xy-plane; the emitter is located at the origin.

assuming the electrons have the Fermi energy. We can now write Eq. (2.9) as

$$r_x(T) = \frac{2\hbar k_F}{eB} \cos\alpha \sin\phi \qquad (2.11)$$

From Eq. (2.11) it follows that $r_x(T)$ takes on a maximum value for $\alpha = 0$, i.e., for those electrons that are injected perpendicular to the crystal surface at the emitter. As also $\partial r_x/\partial\alpha = 0$ for $\alpha = 0$, these electrons will be focused on the surface. Using Eq. (2.5), we get

$$r_y(T) = \int_0^T \hbar k_y/m \, dt = \hbar k_y T/m \qquad (2.12)$$

From the length of the projection of the electron path in the crystal on the xz-plane, we can calculate the time of flight, T, yielding

$$T = (\pi - 2\alpha)m/eB \qquad (2.13)$$

Hence

$$r_y(T) = \frac{\hbar k_F}{eB} (\pi - 2\alpha)\cos\phi \qquad (2.14)$$

In Fig. 2.6 $\vec{r}(T)$ has been plotted in the case of a spherical Fermi surface and a constant magnetic field along the y-axis, for discrete values of α and ϕ. It can be seen from the figure that indeed focusing takes place for extremal values of $r_x(T)$. It can be shown that also for non-spherical Fermi surfaces extremal values of $k_z(0)$ lead to focusing on the crystal surface. So with the double point contact technique the caliper dimensions of the Fermi surface are measured corresponding to extremal values of the wave vector component perpendicular to the crystal surface, of the incoming electrons at the emitter.

In the experiment the point contacts are placed at a distance $L = (r_x^2 + r_y^2)^{1/2}$ from each other. It follows directly from Eqs. (2.11) and (2.12) that the magnetic field strength B_0 at which focusing takes place, is given by

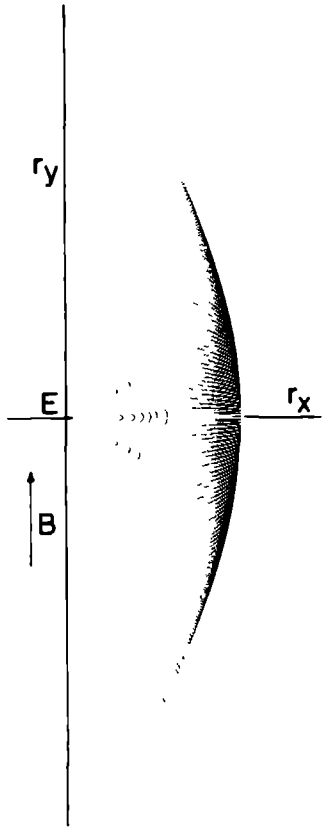

Fig. 2.6
View of the crystal surface with a uniform magnetic field along the y-axis. The points show the positions where the electrons arrive again at the surface after being injected into the crystal at E for discrete values of α and ϕ.

$$B_0 = \frac{2\hbar k_F}{eL} \left(\sin^2\phi + \frac{\pi}{4}\cos^2\phi\right)^{1/2} \qquad (2.15)$$

2.2.3 *Form of the electron focusing signal*

In this section we want to give a more quantitative description of the voltage across the collector as a function of the applied magnetic field. We restrict ourselves to a metal with a spherical Fermi surface and the magnetic field directed perpendicular to the line connecting the point contacts. Taking again the magnetic field along the y-axis and the emitter at the origin, the collector will be on the x-axis at a dis-

tance L from the emitter. We assume furthermore the emitter to be a point source. Because of these conditions $\phi = \frac{\pi}{2}$ and Eq. (2.11) becomes

$$L = \frac{2\hbar k_F}{eB} \cos\alpha \tag{2.16}$$

We assume the collector to be rectangular with dimensions c_x and c_y, as shown in Fig. 2.7; $c_x, c_y \ll L$. For every value of B there will be a solid angle $\Omega = \delta\alpha\delta\phi$, such that electrons, injected into the crystal at

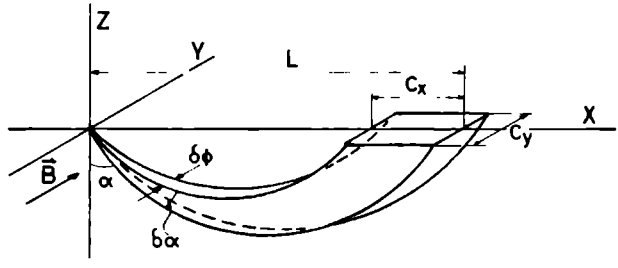

Fig. 2.7 Dimensions of the point contacts. The emitter is located at the origin, and the collector at $[(L - c_x/2) \pm c_x/2, \pm c_y/2]$.

the emitter within this solid angle, can reach the collector. $\delta\alpha$ and $\delta\phi$ are related to the dimensions of the collector as follows

$$L - c_x = \frac{2\hbar k_F}{eB} \cos(\alpha + \delta\alpha) \tag{2.17a}$$

$$\pm\frac{1}{2} c_y = \frac{\hbar k_F}{eB} (\pi - 2\alpha)\cos(\frac{\pi}{2} \mp \frac{1}{2}\delta\phi) \tag{2.17b}$$

Because $c_x, c_y \ll L$, we may assume that $\delta\alpha, \delta\phi \ll 1$, so we can expand the cosine terms in Eqs. (2.17) into a Fourier series, leading to

$$L - c_x = L - L\tan\alpha\delta\alpha - \frac{1}{2}L\delta\alpha^2 + O(\delta\alpha^3) \tag{2.18a}$$

$$\frac{1}{2}c_y = \frac{L(\pi - 2\alpha)}{2\cos\alpha} \frac{1}{2}\delta\phi + O(\delta\phi^3) \tag{2.18b}$$

From this follow expressions for $\delta\alpha$ and $\delta\phi$

$$\delta\alpha \simeq -\tan\alpha + (\tan^2\alpha + 2c_x/L)^{1/2} \qquad (2.19a)$$

$$\delta\phi \simeq \frac{2c_y\cos\alpha}{L(\pi - 2\alpha)} \qquad (2.19b)$$

As can be seen from Fig. 2.8, we can distinguish four different cases:

1. $\alpha \neq 0$. The magnetic field is smaller than the value of the focusing

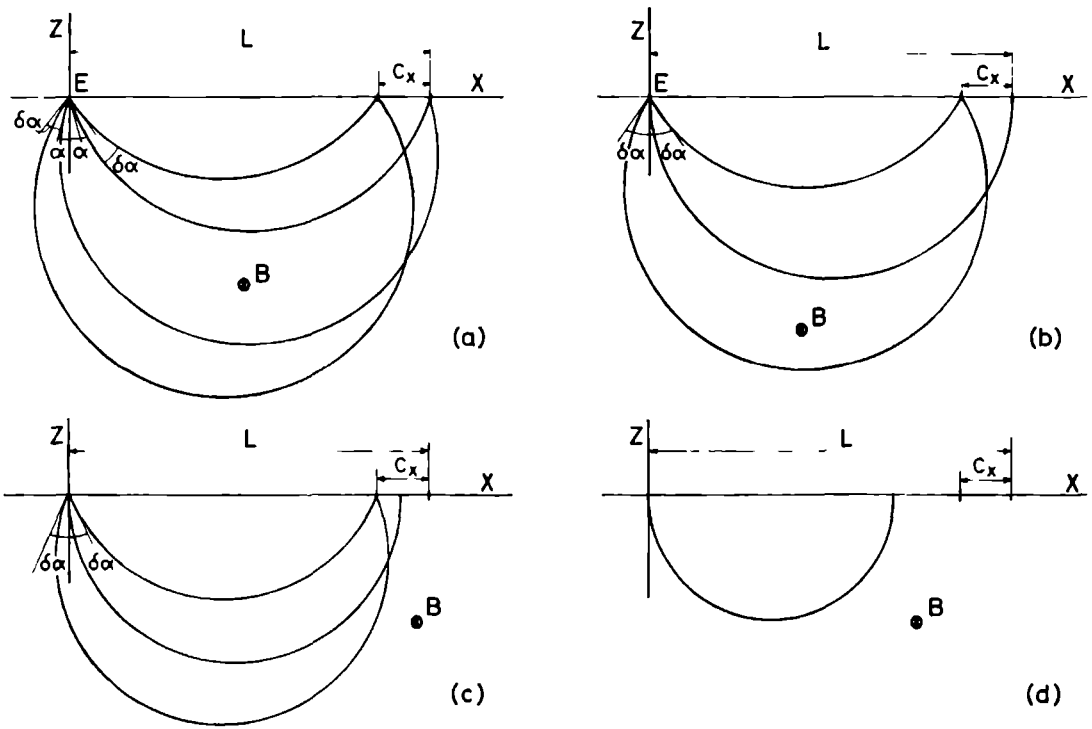

Fig. 2.8 Dependence of $\delta\alpha$ on the applied magnetic field. (a) $B < B_0$; (b) $B = B_0$; (c) $B_0 < B < B_0/(1-c_x/L)$; (d) $B > B_0/(1-c_x/L)$.

field, i.e., $B < B_0 = 2\hbar k_F/eL$. In this case there are two possible solid angles in which electrons can reach the collector. From symmetry arguments $|\alpha|$ and $\delta\alpha$ are the same for these two solid angles, whereas

$$\delta\phi_{\pm} \simeq \frac{2c_y \cos\alpha}{L(\pi \pm 2|\alpha|)} \qquad (2.20)$$

The total solid angle will then be

$$\Omega_1 = \delta\alpha\delta\phi_+ + \delta\alpha\delta\phi_- \simeq \frac{4\pi c_y \cos\alpha}{L(\pi^2 - 4\alpha^2)} \left[-\tan\alpha + (\tan^2\alpha + 2c_x/L)^{1/2}\right] \qquad (2.21)$$

Since, from Eq. (2.16), $\cos\alpha = BeL/2\hbar k_F = B/B_0$, we can write Eq. (2.21) as a function of the applied magnetic field B, yielding

$$\Omega_1 \simeq \frac{4\pi c_y}{L} \left\{\frac{-[1 - (B/B_0)^2]^{1/2} + [1 - (B/B_0)^2(1 - 2c_x/L)]^{1/2}}{\pi^2 - 4\arccos^2(B/B_0)}\right\} \qquad (2.22)$$

2. $\alpha = 0$. The magnetic field now has its focusing value, B_0. We can simply use Eq. (2.22) for the case that $B = B_0$, to get

$$\Omega_2 = \frac{4c_y}{\pi L}(2c_x/L)^{1/2} \qquad (2.23)$$

3. $B_0 < B < B_0/(1-c_x/L)$. Because of its finite dimensions, electrons can still reach the collector. In this case $\delta\alpha$ and $\delta\phi$ are

$$\delta\alpha \simeq [2 - 2(B/B_0)(1-c_x/L)]^{1/2} \qquad (2.24a)$$

$$\delta\phi_+ \simeq \delta\phi_- \simeq 2c_y/\pi L \qquad (2.24b)$$

leading to a solid angle

$$\Omega_3 \simeq \frac{4c_y}{\pi L}[2 - 2(B/B_0)(1-c_x/L)]^{1/2} \qquad (2.25)$$

4. $B > B_0/(1-c_x/L)$. Finally no electrons can reach the collector any more without reflection at the crystal surface. So

$$\Omega_4 = 0 \tag{2.26}$$

Now we can calculate the current through the collector and finally the voltage across the collector as a function of the applied field. The contribution to the collector current from electrons injected into the crystal at an angle α ($\phi = \frac{\pi}{2}$), is given by

$$I_c = \frac{\Omega}{2\pi} I_e \cos\alpha \, e^{(-l_p/\ell)} \tag{2.27}$$

with $I_e \cos\alpha$ the contribution of the electron to the emitter current, assuming that the electrons leave the emitter in all directions inside the the crystal. The exponent gives the chance an electron has to arrive at the collector without collisions, where l_p is the path length in the crystal, and ℓ the mean free path of the electron. l_p can be written as

$$l_p = \frac{L}{\cos\alpha} \left(\frac{\pi}{2} \pm |\alpha|\right) = \frac{B_0 L}{B} \left[\frac{\pi}{2} \pm \arccos(B/B_0)\right] \tag{2.28}$$

where the $\pm$ sign comes from the two different path lengths if $\alpha \neq 0$, as can be seen from Fig. 2.8a. Furthermore, we assume that the collector is a Sharvin junction[15], i.e., the electrons cross the collector ballisticly. This yields a resistance[16]

$$R_S = \frac{4\rho\ell}{3c_x c_y} \tag{2.29}$$

with ρ the resistivity of the metal. Since

$$V_c = I_c R_S = \frac{\Omega}{2\pi} R_S I_e \cos\alpha \, e^{(-l_p/\ell)} \tag{2.30}$$

we can now write down the collector voltage for the four different cases. Substituting Eqs. (2.22), (2.23), (2.25) and (2.26) respectively and Eqs. (2.27) - (2.29) into Eq. (2.30), we get

$$V_c \simeq \frac{8\rho\ell I_e B}{3\pi L c_x B_0} \left\{ \frac{-\left[1 - (B/B_0)^2\right]^{1/2} + \left[1 - (B/B_0)^2(1 - 2c_x/L)\right]^{1/2}}{\pi^2 - 4\arccos^2(B/B_0)} \right\} \times$$

$$\left\{ 2\arccos(B/B_0)\sinh\left[(B_0 L/B\ell)\arccos(B/B_0)\right] + \right.$$

$$\left. \pi\cosh\left[(B_0 L/B\ell)\arccos(B/B_0)\right] \right\} e^{(-\pi L B_0/2\ell B)} \qquad B<B_0 \qquad (2.31a)$$

$$V_c \simeq \frac{8\rho\ell I_e}{3\pi^2 L c_x} (2c_x/L)^{1/2} e^{(-\pi L/2\ell)} \qquad B=B_0 \qquad (2.31b)$$

$$V_c \simeq \frac{8\rho\ell I_e}{3\pi^2 L c_x} \left[2 - 2(B/B_0)(1-c_x/L)\right]^{1/2} e^{(-\pi L/2\ell)} \qquad B_0<B<\frac{B_0}{(1-c_x/L)} \qquad (2.31c)$$

$$V_c = 0 \qquad B>\frac{B_0}{(1-c_x/L)} \qquad (2.31d)$$

If the value of the magnetic field is small compared to the value of the focusing field ($B/B_0 << 1$), we can approximate Eq. (2.31a) by expanding the terms containing (B/B_0). We find

$$V_c \simeq \frac{8\rho\ell I_e B}{3\pi L c_x B_0} \left\{ \frac{(B/B_0)^2(c_x/L)}{4\pi(B/B_0)} \right\} \times \left\{ \frac{e^{(-L/\ell)}}{2(B/B_0)} + \frac{e^{(-\pi B_0 L/B\ell + L/\ell)}}{2\pi - 2(B/B_0)} \right\}$$

$$\simeq \frac{4\rho\ell I_e}{3\pi L^2} e^{(-L/\ell)} \left(\frac{B}{B_0}\right)^2 \qquad B<<B_0 \qquad (2.32)$$

We see that in this limit the collector voltage behaves quadraticly as a function of the applied field. Electrons that are reflected specularly at the crystal surface between the point contacts one or more times, can also add to the collector voltage. This means that the total V_c is a summation over these contributions with the conditions given in Eqs. (2.31) substituting $(n+1)B_0$ for B_0, with n the number of reflec-

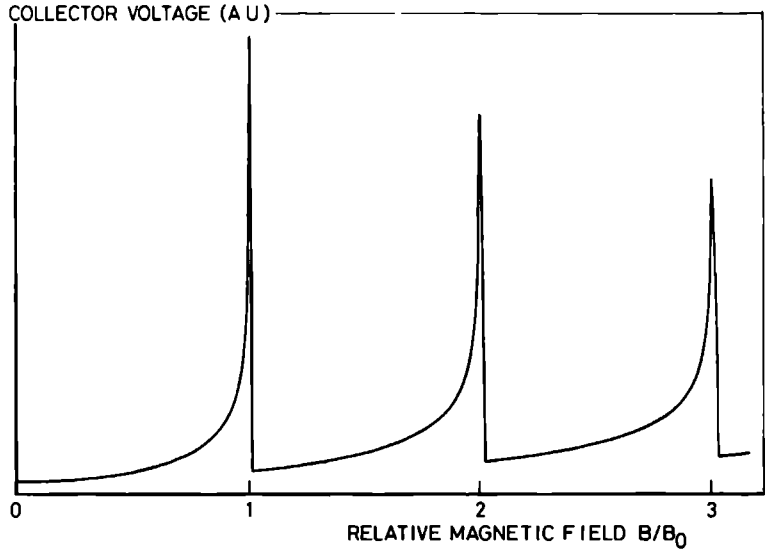

Fig. 2.9 Calculated collector voltage as a function of the applied magnetic field. The ratio of the point contact diameter c_x to the distance between the contacts L equals 0.01, the coefficient for specular reflection q = 0.8.

tions the electron has undergone. Also an extra factor q^n has to be added in Eqs. (2.31), if q is the chance for electrons to reflect specularly from the crystal surface. In Fig. 2.9 Eqs. (2.31) have been plotted with q = 0.8 and $c_x/L = 0.01$.

2.3.1 *Insert and point contacts*

The insert was constructed in such a way that both the point contacts and the sample at low temperatures could be handled from outside (Fig. 2.10). The point contacts consisted of 0.1 mm diameter tungsten wires fixed on a brass lever and bent in such a way that they had some elasticity when touching the crystal surface. The point contact distance was in the order of 0.1 mm. The wires were etched electrolytically in a 1N KOH solution, resulting in sharp points of about 1 um diameter. After immersion in the helium bath the point contacts were spotwelded on the sample surface, using a 90 V battery with a 1 MΩ series resistance. This gave a rather stable contact, also in magnetic fields, with a resistance of order 0.1 Ω. The point contacts could be lifted again from the sample surface in the helium bath, e.g., to rotate the crystal or to renew the contact. Because of the stiffness of the tungsten the wires kept their shape during these operations. The distance between the point contacts varied during cooling down the insert, but this distance change turned out to be rather reproducible in successive measurements. Only after some dozens of spotweldings the point contacts had to be etched again.

Most of the measurements were done in a glass cryostat with an unsilvered tail, so that the direction of the line connecting the point contacts and their distance could be measured in the helium bath. The errors in direction and distance were strongly dependent on the quality of the sight in the bath, but were typically 1^{o} and 0.01 mm respectively.

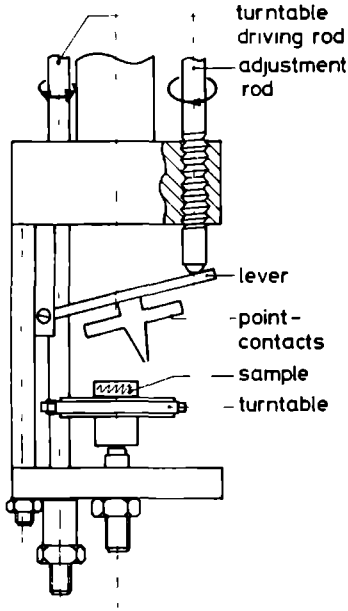

Fig. 2.10
Schematical plot of the insert. The sample is mounted on a gear-wheel and the point contacts on a movable plate. Both sample and point contacts at low temperatures can be handled from outside.

2.3.2 *Electronics*

A schematic of the electronic set-up is given in Fig. 2.11. The emitter current was provided by a function generator and a bipolar power supply/amplifier. Normally a current of 300 mA was used with a frequency of 24 Hz. The voltage across the collector was detected with standard phase-sensitive detection. The magnetic field was produced by a water-cooled iron-core electro-magnet. The field could be rotated through 360^{o} in the horizontal plane, so it was always possible to get the direction of the field perpendicular to the line connecting the point contacts. An analog signal of 15 V/T driven by a Hall probe placed on one of the pole faces, was supplied to the x-axis of an xy-recorder, while the output of the lock-in amplifier was supplied to the y-axis. At signals ranging from 10^{-9} V to 10^{-7} V, the noise was typically 10^{-10} V at zero magnetic field, and 10^{-9} V at 0.4 T.

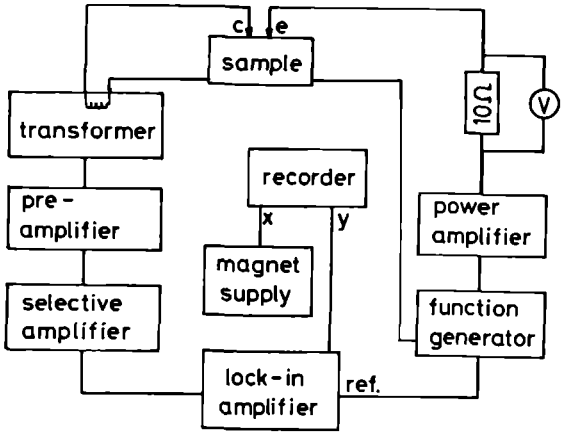

Fig. 2.11
Electronic set-up. The (ac) emitter current is obtained from a function generator and determined by measuring the voltage across a 10 Ω resistance. The collector voltage is measured with phase-sensitive techniques, the reference signal for the lock-in amplifier being the same as the emitter signal.

2.4 *Experimental results*

In this paragraph we discuss the experimental results obtained from two silver single crystals, with surfaces being perpendicular to the [001] and the [011] axes respectively. Silver has an FCC-structure with one conduction electron per atom. The Fermi surface of silver, as for the other two noble metals copper and gold, is entirely contained within the first Brillouin zone and closely related to the free electron Fermi sphere[17]. However, in the <111> directions the surface bulges out to make contact with the zone boundary (Fig. 2.12). For silver these "necks" are rather small, the ratio of the maximal to minimal <111> cross sections being[18] 51. Nevertheless, these necks give rise to a great variety of different electron orbits in a magnetic field.

The samples were single crystals of 6N purity[19], spark-cut from a single crystal rod in the two different orientations. The samples were etched chemically in an NH_3 solution (> 25%) of about 20 ml with 5 to 10 drops of a 40% H_2O_2 solution added. This yielded a shiny surface to the naked eye, terracelike for the (001) crystals, but rather rough for the

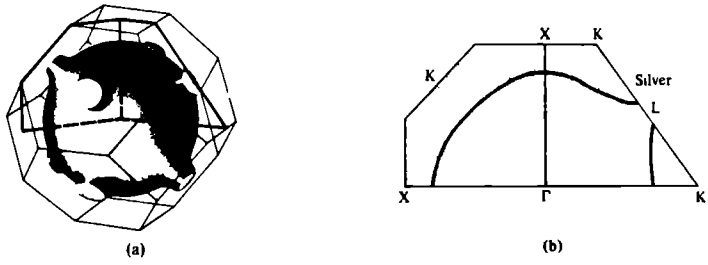

Fig. 2.12 The Fermi surface of Ag. (a) The free electron sphere bulges out in the <111> directions. (b) Detailed cross sections of the surface.

(011) ones. Finally the samples were annealed for eight hours at 850 °C in 10^{-4} torr air[20], yielding a residual resistivity ratio [RRR = R(300 K)/R(4.2 K)] of 15000.

2.4.1 *Silver (001)*

As mentioned above, after chemical etching, the (001) crystals had a terracelike surface. If the etching-solution contained less than about 10 drops of H_2O_2 in 10 ml NH_3, these terraces had rounded corners with the sides more or less along the <100> directions. If more drops H_2O_2 were added, the corners became sharp with the sides now directed along the <110> axes[12,13]. The dimensions of the terraces ranged from 0.05 mm upwards, while the sides had estimated heigths of order 0.01 mm.

Most of the measurements were done at a temperature of 4.2 K, because lowering the temperature had no measurable effect on the intensity of the focusing signals. Fig. 2.13 shows the collector voltage as a function of the applied magnetic field, directed along the [100] axis (a) and the [110] axis (b) respectively. Clearly the peaks can be seen due to direct electron focusing ($\alpha_0,\beta_0,\gamma_0$), and electron focusing after one or more reflections from the crystal surface (α_1,β_1,β_2). The electrons move in k-space over intersections of the Fermi surface perpendicular to the direction of the applied magnetic field. It can be seen from

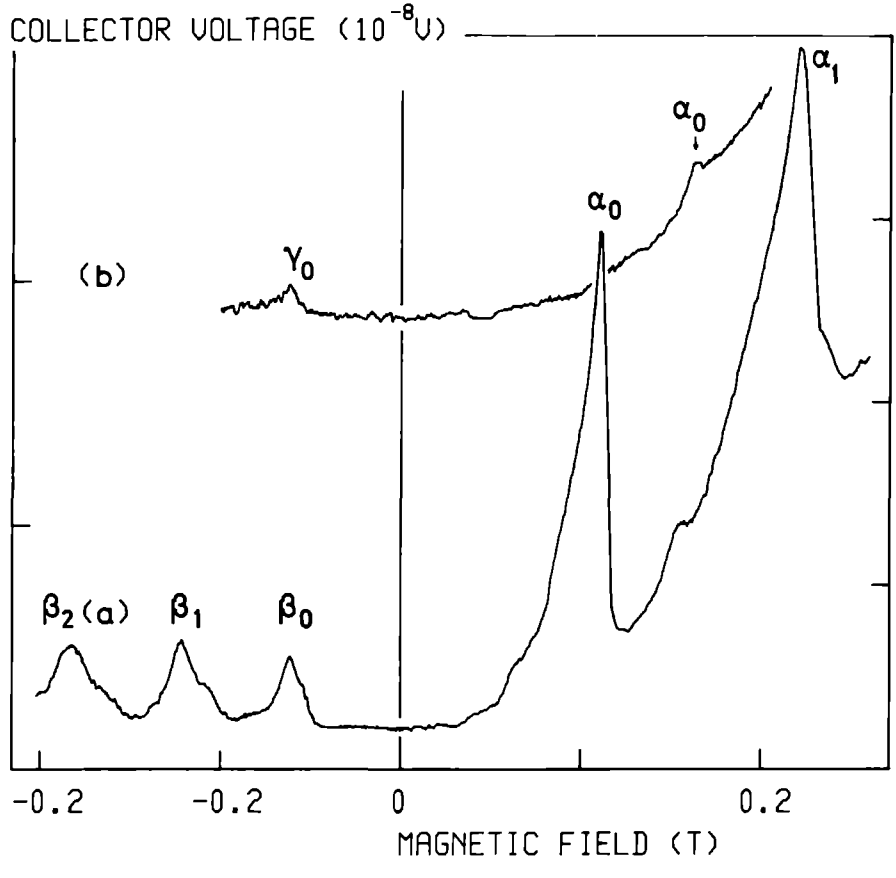

Fig. 2.13 Measured collector voltage as a function of applied magnetic field for Ag (001). (a) If the field is directed along the [100] axis, charged particles on electron "belly" orbits can be observed, focused directly (α_0), or after specular reflection from the crystal surface (α_1), and focusing of particles on hole "four cornered rosette" orbits ($\beta_0, \beta_1, \beta_2$). (b) If the field is directed along the [110] axis, no electron "belly" orbits are possible (the small signal α_0 arises from misalignment), only the hole "dogsbone" orbit can be observed (γ_0).

Fig. 2.14 that perpendicular to the [100] axis two closed orbits exist: an electron "belly" orbit (a) and the hole "four cornered rosette" orbit[21] (b). In Fig. 2.13a these signals are denoted by α and β respectively. As described in section 2.2 this hole orbit is traversed in the opposite direction, so electron focusing on this orbit occurs with the magnetic field also in the opposite direction, as confirmed in Fig. 2.13a. The observation of the "four cornered rosette" with the point contacts perpendicular to the magnetic field is a dramatical example that the velocity component along the field direction in real space need not be uniform, although $|\vec{k}_{\parallel}|$ is constant. For, as the signal in real space is measured along the [010] axis,

$$\vec{r}_{\parallel}(T) = \int_0^T \vec{v}_{\parallel}(t)\, dt = 0 \qquad (2.5)$$

while $\vec{v}_{\parallel} \neq 0$.

Another hole orbit can be seen in Fig. 2.13b, called the "dogsbone"[21]

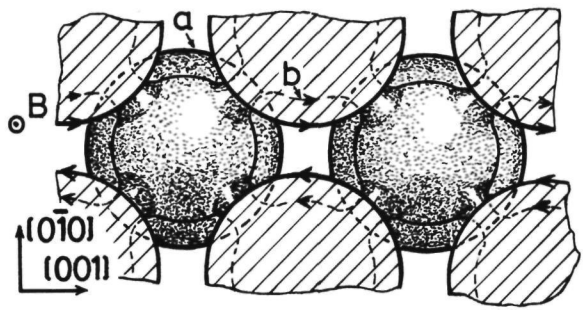

Fig. 2.14 Electron "belly" (a) and hole "four cornered rosette" (b) orbits on the Ag Fermi surface in the repeated zone scheme due to a uniform magnetic field along the [100] direction.

(γ_0). In this direction no electron orbits are possible. The small signal (α_0), that shows up at the right-hand part of the figure, is due to a misalignment of the magnetic field. This means that electrons can still traverse "belly" orbits, but only by crossing one or more necks[22]. This is the reason why the signal shows up at a high field strength

while the amplitude is very small compared to the amplitude of the electron "belly" orbit in the [100] direction.

From Eqs. (2.9) and (2.16) it follows that the component of the k-vector perpendicular to the crystal surface, k_z, can be calculated directly from the value of the focusing field B_0, and the distance between the point contacts L:

$$k_z = \frac{eB_0L}{2\hbar} \qquad (2.33)$$

For the electron "belly" orbit $k_z \equiv k_{001}^{100}(el) = (1.06 + 0.06) \cdot k_F$ was found. Here the superscript stands for the magnetic field orientation, which determines the orientation of the Fermi surface intersections, over which the electron orbits lie; the subscript stands for the direction normal to the crystal surface, which determines the extremal diameter that is measured; (el) denotes that the orbit is electron-like, and k_F is the radius of the free electron Ag Fermi sphere, being equal to $1.20 \cdot 10^8$ cm^{-1}. As can be seen from Fig. 2.14 and Eq. (2.33), the ratio of the extremal k-vectors of the hole "four cornered rosette" and the electron "belly" orbits is, for the same L, equal to the ratio of the measured focusing field strengths. If the belly parts of the orbits agree with the free electron Fermi sphere, this amounts to: $k_{001}^{100}(h)/k_{001}^{100}(el) = 0.51$, where (h) denotes a hole-like orbit. We found experimentally a ratio of 0.55 ± 0.01, indicating a small deviation of the Ag Fermi surface from the free electron sphere.

From the ratio of the intensity of the n^{th}-peak to the $n-1^{th}$- peak the coefficient q for specular reflection can be found. Because of the roughness of the sample surface this ratio varied considerably and therefore we estimate q from our best experimental results with this sample. We found q = 0.8 ± 0.1 both for the electron "belly" and for the hole "four cornered rosette" orbit. Note, that as this belly orbit is an extremal orbit on the Fermi surface ($\vec{B} \perp \vec{L}$), this q is for those electrons moving perpendicular to the crystal surface. The electrons on the "four cornered rosette" orbit, however, have a k-component along the field, being $k_{\parallel} = 0.64 \cdot k_F$. This implies that the electrons to be focused make an angle of about 40° with the normal to the crystal surface.

The silver samples with a (011) surface were after etching shiny to the naked eye, but had a much rougher structure than the (001) samples. For Fermiology, however, a (011) silver surface is very interesting, because the magnetic field can now be directed not only along the [100] and [110] axes, but also along the [111] axis, where the electron "neck" orbit should show up. However, we were not able to observe this orbit, nor the hole "four cornered rosette" orbit with this sample. Electrons on this orbit that are focused in the (011) sample onto the collector, start at the emitter on the neck parts of the Fermi surface, because their wave vector component perpendicular to the magnetic field is in the [011] direction, as can be deduced from Fig. 2.14. There are probably insufficient electrons on these necks at the emitter, to observe their focusing at the collector. That we indeed were able to observe the "four cornered rosette" and the "dogsbone" orbits with the (001) sample, indicates that the electrons in the bulk material have a real chance to cross the necks on the Fermi surface, although there the Fermi velocity is smallest and hence the electron-phonon coupling greatest[23].

In Fig. 2.15 experimental results have been plotted for three directions of the applied magnetic field: the [110], [111], and [100] direction respectively. In the [100] and [111] directions electron "belly" orbits can be seen in the right-hand part of the figure; in the [110] direction no extremal electron orbit exists, in agreement with the model of the Ag Fermi surface[17]. The small signal at the right is due to misalignment of the applied field, through which electron "belly" orbits are still possible, however, by crossing one or more necks[22], as has been noted in the previous section. Note the great difference between the [100] and [111] signal intensities. We will come back to this in the next section. Contrary to our expectations from the quality of the sample surface, the specularity coefficient is rather high, though not constant for the different crystal directions. We found q = 0.9 and 0.7 for the electron "belly" orbits in the [100] direction and the [111] direction respectively. When the magnetic field was applied in other directions, often very low specularity coefficients (< 0.3) were meas-

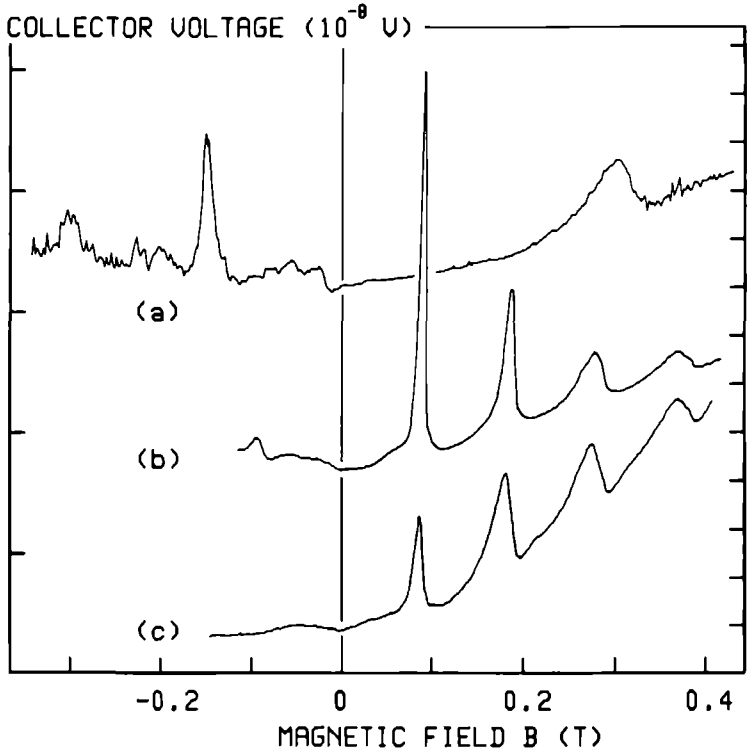

Fig. 2.15 Measured collector voltage as a function of applied magnetic field for Ag (011); electron orbits are displayed on the right-hand part of the figure, and hole orbits on the left-hand part. (a) B // [110] showing the hole "dogsbone" orbit, at the right a small electron "belly" orbit can be seen due to misalignment of the magnetic field; (b) B // [111] showing an electron "belly" orbit and the hole "six cornered rosette" orbit; (c) B // [100] showing an electron "belly". Note the great intensity difference between the signals of the electron "belly" orbits in (b) and (c). Note also the different voltage scales for the right- and left-hand plots.

ured for electrons on "belly" orbits. This is in contrast to the results obtained with the (001) sample, where for different directions roughly the same coefficients for specular reflection were measured. Probably, this is caused by the quality of the crystal surface, for as it has been etched chemically, some crystal directions will be flatter than others. For the hole orbit in the [110] direction we found $q = 0.3$. In the [111] direction no hole specularity coefficient was recorded. In table 2.1 the reflection coefficients of metals and semi-

TABLE 2.1 Coefficients for specular reflection from the crystal surface measured with the double point contact technique.

metal	B //	surface	q_{el}	q_h	Ref.
Bi	-	$\perp c_3$-axis	0.75	-	4
Bi	-	$\perp c_3$-axis	0.6-0.8	-	5
Sb	-	$\perp c_3$-axis	0.8	-	6
W	-	(110)	0.65	0.65	7
W	[100] - [112]	(100)	0.1	-	7
W	-	(110)	0.6	0.6	8
W	-	(001)	0-0.25	0-0.7	8
W	-	(110)	0.55	0.55	9
Cu	[001]	(110)	0.35	-	7
Cu	[$\bar{1}$11]	(110)	0.35	-	11
Cu	[010]	(100)	0.45	-	11
Ag	[010]	(001)	0.7	-	12
Ag	-	(011)	0.6	-	12
Ag	[010]	(001)	0.8	0.8	13
Ag	[010]	(001)	0.8	0.8	24
Ag	[010]	(011)	0.9	-	24
Ag	[111]	(011)	0.7	-	24
Ag	[110]	(011)	-	0.3	24
Al	[21$\bar{1}$]	(011)	-	0.3	14

metals are summarized, measured with this technique.

As can be seen from Fig. 2.15, both in the [110] and in the [111] directions, hole orbits show up; the "dogsbone" orbit again in the [110] direction, and the "six cornered rosette" orbit[21] in the [111] direction. Different extremes of the "dogsbone" orbit are measured in the (001) surface and the (011) surface samples. This can be seen from

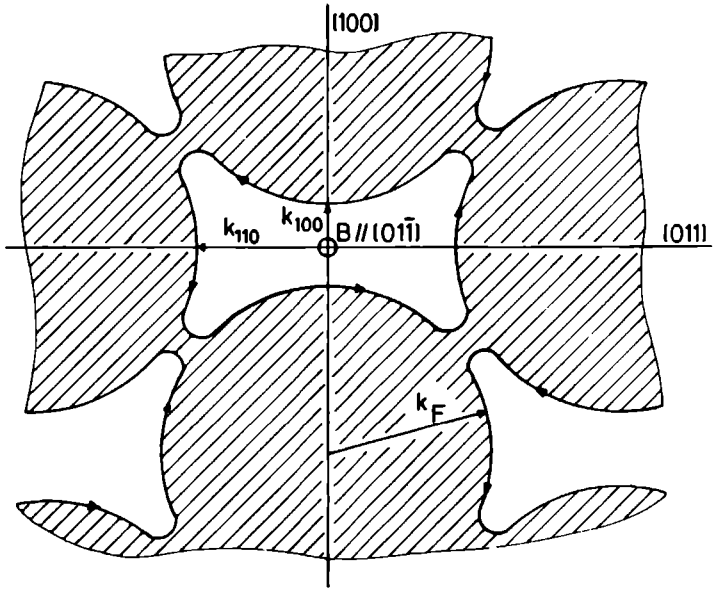

Fig. 2.16 The "dogsbone" orbit in k-space in the repeated zone scheme, showing the different extremes that can be measured with different crystal surface orientations.

Fig. 2.16, where the extremes are denoted by k_{100} and k_{110} respectively. If the belly parts of the orbit were on the free electron Ag Fermi sphere, then $k_{011}^{110}(h) = 0.81 \cdot k_F$, where again the subscript and the superscript stand for the orientation of the crystal surface and of the applied magnetic field respectively. From our measurements we have $k_{011}^{110}(h) = (0.79 \pm 0.02) \cdot k_F$, in good agreement with the free electron approximation.

Fig. 2.17 shows two intersections of the Ag Fermi surface in the repeated zone scheme perpendicular to the $[11\bar{1}]$ axis: one through the origin showing an electron "belly" orbit, and one through $[\frac{11\bar{1}}{666}]$ showing the

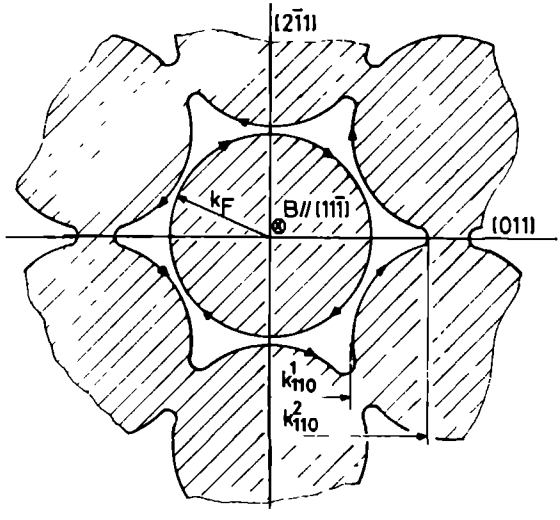

Fig. 2.17
Electron "belly" (a) and hole "six cornered rosette" (b) orbits on the Ag Fermi surface, with the magnetic field along the [111] direction.

hole "six cornered rosette" orbit. The electron "belly" orbit is approximately circular with radius k_F. We found $k^{111}_{011}(el) = (1.00 \pm 0.03)\cdot k_F$. As can be seen from Fig. 2.17, with the (011) crystal two extremes exist in the hole "six cornered rosette" orbit (k^1_{011} and k^2_{011}). From the arguments given above it is clear that we could observe only the smallest one (k^1_{011}). The signal plotted in Fig. 2.15b corresponds to k^1_{011} as can be seen from the signal form: first a steep rise and then a slower fall, opposite to the peaks arising from electron "belly" orbits (Figs. 2.15b and 2.15c). If the belly parts of the orbit were on the free electron Fermi sphere, this extreme would be: $k^{111}_{011}(h) = 0.83\cdot k_F$. We found $k^{111}_{011}(h) = (0.96 \pm 0.02)\cdot k_F$. So in this vicinity the curvature of the real Ag Fermi surface is smaller than the curvature would be in the free electron approximation. In table 2.2 the measured extremes of cross sections of the Ag Fermi surface have been summarized.

TABLE 2.2 Comparison of measured and, for the free electron model, calculated wave vectors; $k_z(el)$ and $k_z(h)$ are the components of the momentum perpendicular to the crystal surface for electron and hole orbits respectively.

sample	B //	$k_z(el)/k_F$ meas	$k_z(el)/k_F$ calc	$k_z(h)/k_F$ meas	$k_z(h)/k_F$ calc
Ag (001)	[100]	1.06 ± 0.06	1	0.58 ± 0.06	0.51
Ag (011)	[110]	-	-	0.79 ± 0.02	0.81
	[111]	1.00 ± 0.03	1	0.96 ± 0.02	0.85

We conclude that for both samples the coefficient for specular reflection along symmetry axes is the same, namely, $q = 0.8 \pm 0.1$, except for the hole "dogsbone" orbit from the (011) sample where only 0.3 was found. The measured Fermi momenta agree in almost all measured crystal directions with those for the free electron Ag Fermi sphere. However, the measurement of the distance between the point contacts, which was necessary to fix the Fermi momenta, was rather inaccurate, and limits the accuracy of the measurements. However, in section 2.4.4 it will be seen, that with this technique even small differences in the shape of the Fermi surface can be measured.

2.4.3 *Electron focusing as a function of the point contact distance*

Eq. (2.31b) gives the collector voltage as a function of, among other things, the distance between the point contacts. In Fig. 2.18 this relation has been plotted for two collector diameters: $c_x = 0.1$ μm, using Eq. (2.29), corresponding to a contact resistance $R_S = 0.14$ Ω (upper curve), and $c_x = 0.17$ μm, corresponding to $R_S = 0.05$ Ω (lower curve). Normally, the measured point contact resistances were between these

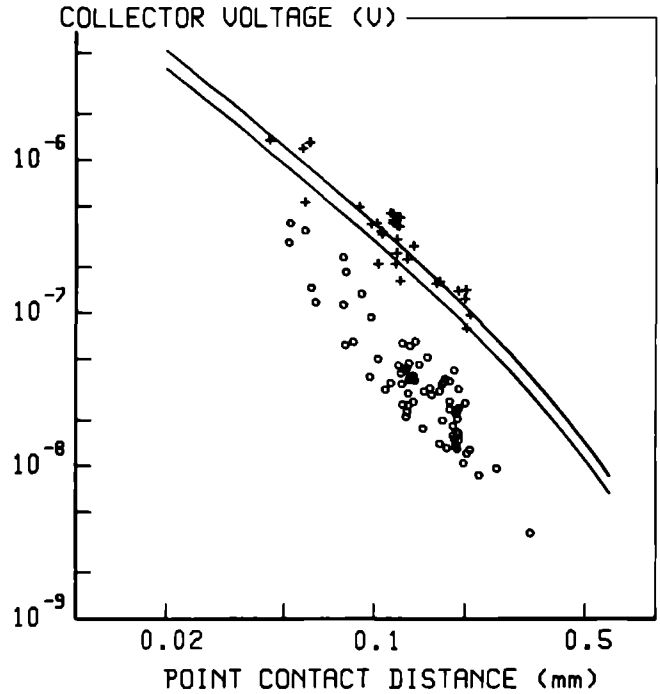

Fig. 2.18 Collector voltage as a function of the point contact distance. Solid lines: Eq. (2.31b), with I_e = 300 mA, mfp = 700 μm, and c_x = 0.1 μm (upper curve) and 0.17 μm (lower curve) respectively (see text). The circles show the measured intensities of the direct focusing signals with B // [100]; the crosses show the measured intensities with B // [111] and B ≈ // [211].

values. In both curves the emitter current, I_e, equals 300 mA, and the electron mean free path, ℓ = 700 μm. Also the measured intensities of the direct electron focusing peak have been plotted, both for the (001) and for the (011) samples, corrected for an emitter current of 300 mA. The circles refer to measurements with the applied magnetic field in the [100] direction, while the crosses give the results obtained with the field in the [111] and near the [211] directions. Although the variety in the measured values is larger than the distance between the two curves, both the direction and the order of magnitude are correct. We

have to realize that Eq. (2.31b) is correct for the approximation of an ideal Sharvin junction[15], a spherical Fermi surface, and a flat crystal surface. As these conditions are generally not satisfied, e.g., because of a dirty contact causing a partial resistance barrier; a non-spherical Fermi surface; or an oblique contact area, we might expect this variety in intensities. However, we may conclude that this model is rather good as an upper limit. Note the great difference in amplitude between the [100] and the [111]/[211] signals, the last ones lying even higher sometimes than the calculated curves. This amplitude difference has been measured with the same sample as well, as can be seen from Fig. 2.15b,c. We can explain this difference qualitatively by looking at the shape of the Ag Fermi surface. As the group velocity of the electrons [Eq. (2.1)] is always normal to the Fermi surface, a bump on this surface makes the deviation in the velocity in real space larger than the deviation in momentum (Fig. 2.19a), so that the solid angle in which electrons are able to reach the collector is smaller, and therefore the

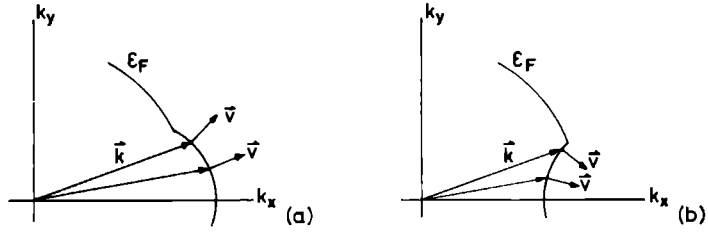

Fig. 2.19 Influence of the shape of the Fermi surface on the intensity of the EF signal. Because the electron velocity is normal to the Fermi surface, the focusing solid angle is reduced by a bump (a), and increased by a dip (b).

collector signal is smaller. On the contrary, flatter parts or dips on the Fermi surface have a focusing effect on the movements of the electrons (Fig. 2.19b). The extremal orbits in the <100> directions go over those bumps, so the measured collector signal will be smaller than that calculated for a spherical Fermi surface. However, the extremal orbits in the <111> directions go over more spherical parts of the Fermi surface, while in the neighbourhood of the necks the Fermi surface is even

oppositely curved (Fig. 2.12), resulting in the great collector voltages. Also in the shape of the collector signal information can be obtained about the shape of the Fermi surface. Comparison of Fig. 2.15 with the calculated curve plotted in Fig. 2.9, shows that also the form of the [111] signal agrees more with theory than the form of the [100] signal.

Apart from the fact that the signals are broadened by the shape of the Fermi surface, the width of the decreasing parts of the signals says something about the diameter of the point contacts, as can been seen from Eq. (2.31c). From the width of these decreasing parts it follows that the point contact diameters are in the order of 10 μm, in violent contrast with the diameters found for Sharvin junctions with the typical contact resistances, yielding ~0.1 μm. We will come back to this in chapter IV.

We may conclude, however, that the extremal orbits on the Ag Fermi surface perpendicular to the <111> directions, correspond more to the free electron approximation than extremal orbits perpendicular to the <100> directions.

2.4.4 *Variation of the direction of the applied magnetic field*

So far the applied magnetic field had been oriented perpendicular to the line connecting the point contacts. If the field direction is varied with respect to this line, electron focusing can still occur. However, now only electrons that are injected at the emitter with a particular velocity component parallel to the field direction, can reach the collector. This means that the electrons that are focused, no longer traverse extremal orbits on the Fermi surface. The section in which the focusing electron orbit lies on the Fermi surface, is not only shifted with respect to the extremal one, but also rotated, because it is always normal to the direction of the applied field. The point contacts, however, stay in the same position on the crystal surface. Fig. 2.20a shows the projection on the (001) plane of the orbit on the Fermi surface if the field direction deviates an angle θ from the [100] axis, the point contacts being oriented along the [010] axis. The rela-

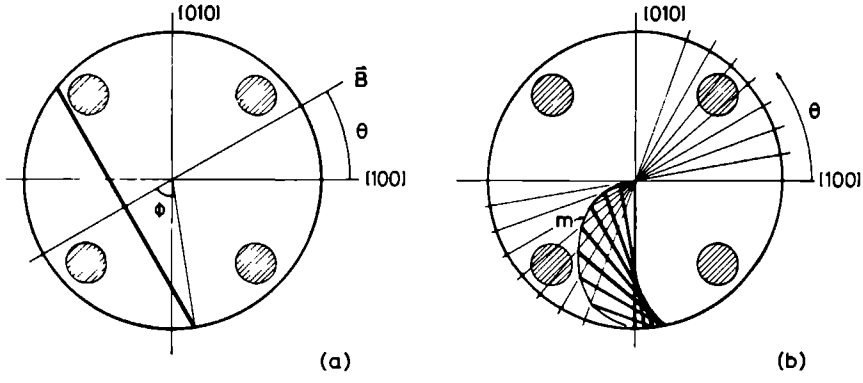

Fig. 2.20 Projection on the (001) plane of focusing electron orbits on the Fermi surface if the applied magnetic field is not perpendicular to the line connecting the point contacts. (a) Relation between θ and φ given by Eq. (2.34); (b) as only half of the orbit is traversed, with Ag (001) the electrons are not influenced by the necks on varying θ. The measured extremes lie on the curve m.

tion between θ and φ can be found from Eqs. (2.11) and (2.14) for α = 0, yielding

$$\tan\theta = r_y(T)/r_x(T) = \frac{\pi}{2}\tan\phi \qquad (2.34)$$

As only half of the orbit is traversed in the case of electron focusing with point contacts, the electrons are not influenced by the necks on the Fermi surface when varying the field direction, if the crystal surface is perpendicular to the [001] axis (Fig. 2.20b).

Fig. 2.21 shows measured and calculated results as a function of θ with the point contacts oriented along the [010] axis. In Fig. 2.21a the measured focusing field strengths (circles) have been plotted together with the values one should get in the case of a spherical Fermi surface. From the plot it is clear that the Fermi surface is rather spherical. Only in the [100] direction (θ = 0) there is a small deviation from the calculated curve. As described already in the previous section, the real Ag Fermi surface is not perfectly spherical in the

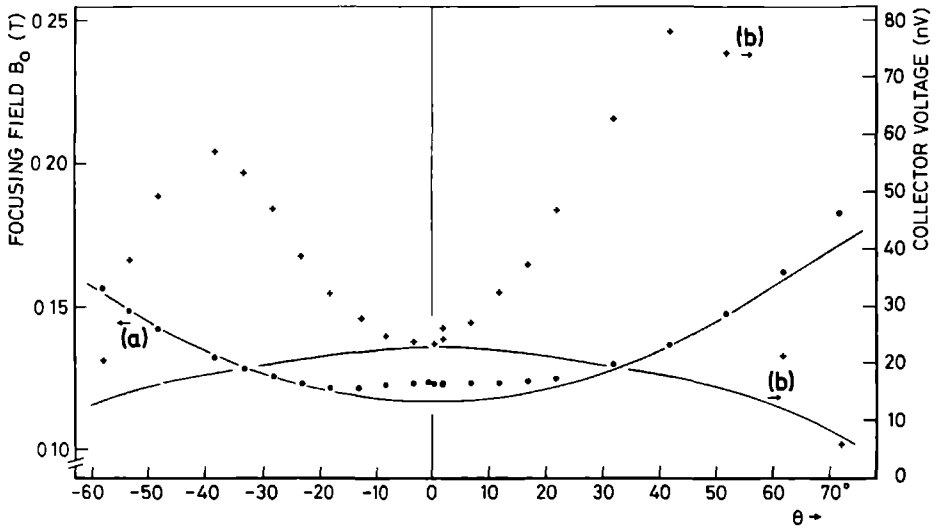

Fig. 2.21 Measured (points) and calculated (curves) results as a function of the direction of the applied magnetic field with respect to the line connecting the point contacts. (a) Strength of the focusing field (circles); (b) intensity of the electron focusing peak (crosses).

<100> directions. In Fig. 2.21b the intensities of the electron focusing peak have been plotted (crosses). Although these results have been measured with the same point contacts, they don't agree at all with those calculated for a spherical Fermi surface. The plot shows how sensitive the electron focusing experiment is to the form of the electron orbits. For, like the <111> orbits described in the previous section, the non-extremal orbits for $\theta \sim 45^{\circ}$ lie on more spherical parts of the Fermi surface, giving rise to an increase of the collector signal. Fig. 2.22 shows that for $\theta = 0$ (a) the signal has not only a smaller intensity but is also much broader than the signal with $\theta = 45^{\circ}$ (b). The last one agrees more with the result calculated for a spherical Fermi surface (Fig. 2.9) and also with the measured [111] signal (Fig. 2.15b). It is obvious that for a quantitative explanation of the observed intensities the electrons have to be followed over their entire orbits on the Fermi surface. This course is not pursued, however, it is clear from

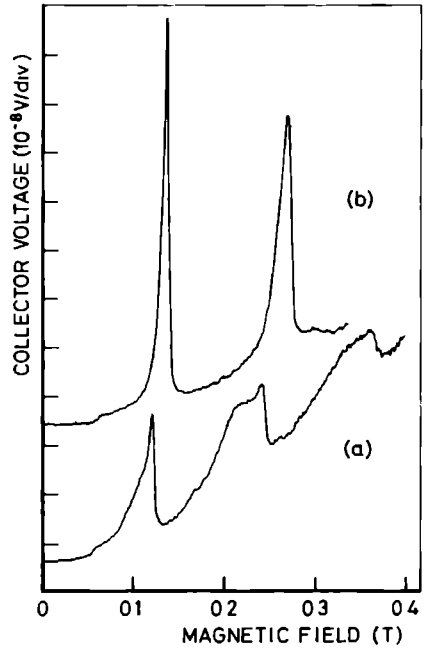

Fig. 2.22
Measured collector voltage as a function of the applied field directed perpendicular to the line connecting the point contacts (a), and at an angle of 45° (b). Note, besides the difference in amplitude, also the difference in shape.

Fig. 2.20 that with this method detailed information can be obtained about any closed orbit on the Fermi surface.

2.4.5 *Electron focusing as a function of applied dc voltage*

We argued above that the electrons injected into the crystal at the emitter, will thermalize immediately because of the high currents used. The current being in the order of 300 mA, lead with a typical emitter resistance of about 0.1 Ω, to an emitter voltage of about 30 mV. Electrons thus injected, have energies far above the energy for spontaneous phonon emission (~10 meV)[25]. However, if the electrons are injected with lower energies, they should be able to keep this energy, or part of it, on their way through the crystal. The electron mean free path is not only determined by elastic scattering with impurities (ℓ_{imp}), but also by inelastic scattering with phonons (ℓ_{ep}). Using Matthiessen's rule the total scattering length, ℓ, can be written as

$$1/\ell = 1/\ell_{imp} + 1/\ell_{ep} \qquad (2.35)$$

Only the electron-phonon length, ℓ_{ep}, will be energy dependent, being at low energies inversely proportional to the energy to the third power[26]:

$$\ell_{ep} = C/\varepsilon^3 \qquad (2.36)$$

The proportionality constant depends, among other things, on the kind of metal. Fig. 2.23 shows the recorder output of the collector voltage as a function of applied dc emitter voltage at B = 0 and B = B_0 respectively, without shifting the recorder pen between the two voltage sweeps. The modulation voltage (3.4 mV peak-to-peak) has also been indicated. The distance between the point contacts was 0.19 mm, and the magnetic field was directed along the [010] axis. Clearly a bump can be seen at voltages smaller than about 5 mV in the upper curve. Obviously, the electron-phonon length, lep, is large enough to allow electron focusing at these low energies. Because the path length l_p is proportional to the distance between the point contacts L, the width of the bump will depend a little on L. We can estimate the constant C in Eq. (2.36) by

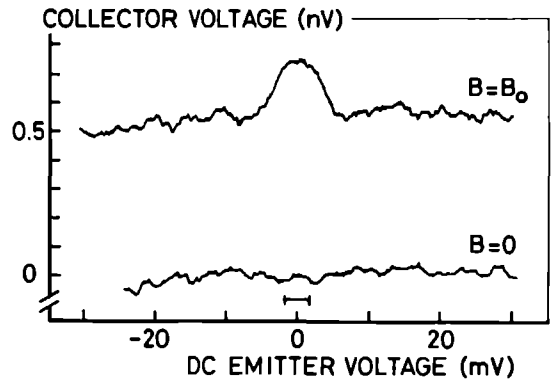

Fig. 2.23 Recorder output of the collector voltage as a function of applied dc emitter voltage at zero magnetic field (lower curve) and the focusing field (upper curve). The modulation voltage (3.4 mV peak-to-peak) has been indicated as well.

fitting the expression found for the collector voltage [Eq. (2.31b)] to the measured bump using the energy dependent electron mean free path [Eq. (2.35)]. We found $C = (2 \pm 1) \cdot 10^4$ $\mu m/meV)^3$. This is a very crude estimate, firstly because C is calculated from only one measurement, and secondly because the point contacts did not consist of the same material as the single crystal; the point contact material also contributes to the energy dependence of the electron-phonon scattering length[26]. At high applied dc emitter voltages the electrons loose their energy so close to the emitter that the scattering area can be considered as a point source. Next the electrons, being at the Fermi energy, are scattered by impurities only. The impurity scattering length, ℓ_{imp}, is large enough that the electrons can reach the collector without further scattering.

Actually, the measured collector voltages presented in the previous sections, have to be increased by a factor 1.3, as can be seen from Fig. 2.23. However, the spread in the measured intensities and the deviation of the [100] signals from the calculated curves, as indicated in Fig. 2.18, are too large to explain with this factor. In any case, Fig. 2.23 shows that it is possible to observe electrons with an energy above the Fermi energy in a metal single crystal on orbits of constant energy up to about 5 meV.

2.5 *Concluding remarks*

We conclude that we have observed the magnetic focusing of electrons in a silver single crystal by means of point contacts. Direct electron focusing was measured for different orbits on the Ag Fermi surface, as well as focusing after one or more specular reflections from the crystal surface. We found a coefficient for specular reflection of 0.8 ± 0.1, independent of the orientation of the crystal surface, for orbits lying in planes perpendicular to the <100> and <111> directions. This indicates that, at least in these directions, the crystal surface is relatively flat on an atomic scale, in spite of the fact that the surface seemed rough under a microscope. The experimentally obtained diameters of the electron orbits are in good agreement with a spherical Fermi sur-

face. However, there is a large variety in the intensity and shape of the collector signals for different orbits on the Ag Fermi surface, showing that with this technique even very small changes in the shape of the Fermi surface can be detected.

We are grateful to Ing. T. J. Gortenmulder and late Dr. B. Knook of the Kamerlingh Onnes Laboratory, Leiden, for growing the silver single crystal from the melt, and Ir. L. W. M. Schreurs for orienting and spark-cutting the sample. This work is part of the research program of the Stichting voor Fundamenteel Onderzoek der Materie and was made possible by financial support from the Nederlandse Organisatie voor Zuiver Wetenschappelijk Onderzoek.

References

1. Yu. V. Sharvin, Zh. Eksp. Teor. Fiz. 48, 984 (1965) [Sov. Phys. -JETP 21, 655 (1965)].
2. Yu. V. Sharvin, and L. M. Fisher, ZhETF Pis. Red. 1, 54 (1965) [JETP Lett. 1, 152 (1965)].
3. Yu. V. Sharvin, and N. I. Bogatina, Zh. Eksp. Teor. Fiz. 56, 772 (1969) [Sov. Phys. -JETP 29, 419 (1969)].
4. V. S. Tsoi, ZhETF Pis. Red. 19, 114 (1974) [JETP Lett. 19, 70 (1974)].
5. V. S. Tsoi, Zh. Eksp. Teor. Fiz. 68, 1849 (1975) [Sov. Phys. -JETP 41, 927 (1975)].
6. V. S. Tsoi, and I. I. Razgonov, Pis'ma ZhETF 23, 107 (1976) [JETP Lett. 23, 92 (1976)].
7. V. S. Tsoi, and I. I. Razgonov, Pis'ma ZhETF 25, 30 (1977) [JETP Lett. 25, 26 (1977)].
8. V. S. Tsoi, and I. I. Razgonov, Zh. Eksp. Teor. Fiz. 74, 1137 (1978) [Sov. Phys. -JETP 47, 597 (1978)].
9. A. A. Mitryaef, O. A. Panchenko, I. I. Razgonov, and V. S. Tsoi, Surface Sience 75, L376 (1978).
10. E. L. M. Payens, doctoral thesis.
11. P. J. M. W. L. Birker, H. van Kempen, and P. Wyder, J. Physique C6, 1128 (1978).
12. V. S. Tsoi, J. Bass, P. A. M. Benistant, H. van Kempen, E. L. M. Payens, and P. Wyder, J. Phys. F: Metal Phys. 9, L221 (1979).
13. P. A. M. Benistant, doctoral thesis.
14. P. A. M. Benistant, H. van Kempen, and P. Wyder, to be published.
15. A Sharvin junction is a metallic junction in the extreme Knudsen regime ($\ell/a \gg 1$, with ℓ the mean free path and a the contact radius). See Ref. 1.
16. A. G. M. Jansen, A. P. van Gelder, and P. Wyder, J. Phys. C: Solid St. Phys. 13, 6073 (1980).
17. D. Shoenberg, and D. J. Roaf, Phil. Trans. Roy. Soc. 255, 85 (1962).
18. M. R. Halse, Phil. Trans. Roy. Soc. A 265, 507 (1969).

19. Cominco ltd., Trail, B. C., Canada.
20. A. C. Ehrlich, J. Mat. Science 9, 1064 (1974).
21. D. Schoenberg, Phil. Trans. Roy. Soc. A 255, 85 (1962).
22. A. B. Pippard, in Documents on Modern Physics, Gordon and Breach (1965).
23. B. Lengeler, W. R. Wampler, R. Bourassa, K. Mika, K. Wingerath, and W. Uelhoff, Phys. Rev. B 15, 5493 (1977).
24. Results from measurements described in this paper.
25. Yu. N. Shalov, and I. K. Yanson, Fiz. Nizk. Temp. 3, 99 (1977) [Sov. J. Low Temp. Phys. 3, 48 (1977)].
26. A. G. M. Jansen, F. M. Mueller, and P. Wyder, Phys. Rev. B 16, 1325 (1977).

ABSTRACT

In this chapter we report the observation of electron focusing in an aluminium single crystal with a (011) surface. Extremal orbits in different directions on the second zone Fermi surface have been observed. For the given crystal surface the coefficient for specular reflection was estimated to be 0.3.

In 1974 V.S. Tsoi[1] introduced a method using point contacts, to observe the magnetic focusing of electrons in metal single crystals on particular orbits of the Fermi surface. Many metals have been examined in this way already: e.g., bismuth[1], antimony[2], tungsten and copper[3], and silver[4]. We present for the first time electron focusing (EF) in aluminium.

The principle of this method can be seen in Fig. 3.1: through one

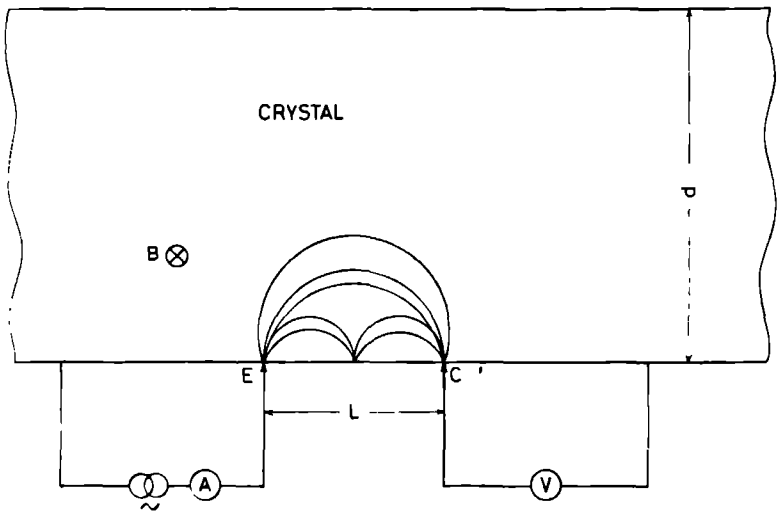

Fig. 3.1 Electron focusing (EF) in a pure metal single crystal by a homogeneous magnetic field with the use of point contacts.

point contact, the emitter, a current flows and a homogeneous magnetic field, parallel to the surface, bends the injected electrons so that they follow paths over the Fermi surface in a plane perpendicular to the direction of the applied field. At a particular field strength the electrons will be focused on the other point contact, the collector, leading to a voltage peak. Also at multiple field strengths voltage peaks can be recorded due to one or more specular reflections of the

electrons at the crystal surface between the point contacts.

Aluminium is a trivalent metal with a monatomic fcc Bravais lattice with a Fermi surface very close to the free electron surface. In this case the free electron Fermi sphere completely encloses the first Brillouin zone, leaving a hole surface in the second Brillouin zone and an electron surface in the third zone[5] (Fig. 3.2). This gives rise to many different types of orbits an electron can traverse in an applied magnetic field. From Fig. 3.3 it can be seen that electrons that are injected perpendicular to the crystal surface at the emitter, will be focused on

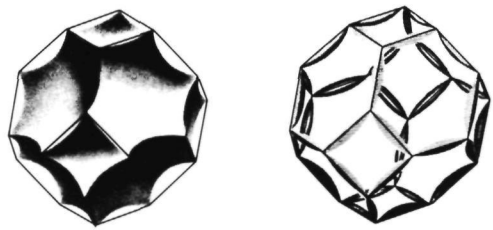

Fig. 3.2 The Fermi surface of Al. (a) Portion of the free electron sphere in the second zone translated back into the first zone. The surface encloses holes. (b) Portion of the free electron sphere in the third zone translated back into the first zone. The surface encloses particles.

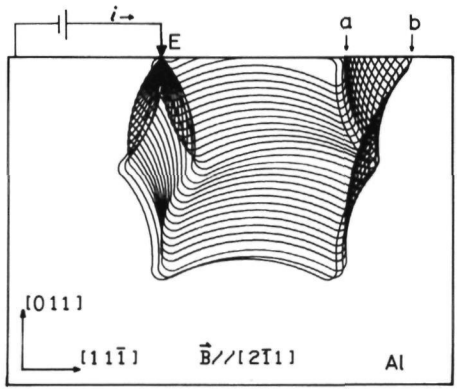

Fig. 3.3
Trajectories of charged particles in aluminium in a plane perpendicular to the [21$\bar{1}$] direction. Note that electrons injected perpendicular to the crystal surface at the emitter (E) are focused on the surface (a and b).

the collector. With this method the caliper dimensions of orbits on the Fermi surface can be measured, by choosing the direction of the line connecting the point contacts and the direction of the applied magnetic field with respect to the crystal axes.

3.2 *Sample and point contact preparation*

The sample was an Al single crystal[6] of 6N purity, spark-cut with the surface perpendicular to the [011] direction. The sample was etched chemically in a KOH solution and annealed in vacuum for one hour at 500 °C. As the sample was etched chemically only, the surface had a hilly shape. The point contacts were 0.1 mm diameter tungsten wires with sharp points of about 1 μm diameter etched electrolytically in a 1N KOH solution. The insert was constructed in such a way that the point contacts could be placed on the sample surface and lifted from it in the helium bath. The sample itself could be rotated with respect to the point contacts also at low temperatures. The point contacts were spotwelded on the sample surface, using a 150 V battery with a 1 MΩ series resistance. Normally three or four attemps had to be made before a stable, low Ohmic contact with a resistance varying from 0.07 to 0.2 Ω was achieved. An ac current of about 200 mA was sent through the emitter and the voltage across the collector was measured with standard phase sensitive and lock-in techniques. The magnetic field was provided by a water-cooled iron-core electro-magnet, which could be rotated through 360° in the horizontal plane. Because the tail of the used cryostat was left unsilvered, it was possible to measure the direction and length of the line connecting the point contacts.

3.3 *Experimental results*

Reproducible results have been obtained from many different places on the sample surface. However, only orbits on the second Brillouin zone have been observed. Probably the intensity of signals caused by electrons on the third Brillouin zone was too small to be detected, because

of the sharp curvature of the third zone surface (Fig. 3.2b). In Figs. 3.4a - 3.4c measured collector voltages are shown as a function of applied magnetic field, the field directed along the $[01\bar{1}]$, $[11\bar{1}]$ and $[21\bar{1}]$ axis respectively. Also the sections of the second zone Fermi

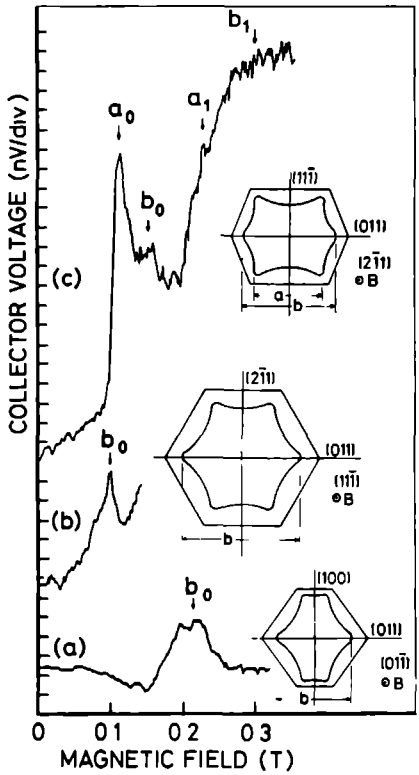

Fig. 3.4
Experimental results with the magnetic field oriented along the $[01\bar{1}]$ (a), the $[11\bar{1}]$ (b) and the $[21\bar{1}]$ (c) axis respectively. Note the different shapes of the signals: hole-like signals (a_0, a_1) with a relatively steep rise due to local minima in the diameters of the electron orbits on the Fermi surface, and electron-like signals (b_0) with a relatively steep fall due to local maxima.

surface have been drawn for these orientations of the magnetic field. The distances between the point contacts were 0.08, 0.2, and 0.1 mm respectively. Note that the shape of the signals differs a lot for the different field orientations. This can be understood by realizing that what is measured are the dimensions parallel to the crystal surface of the electron orbits, as has been indicated in Fig. 3.4. It can be shown[7], that a (local) maximum leads to a signal as a function of applied magnetic field with a quadratic like rise and a steep fall. In the same way it can be derived, that a local minimum gives a steep rise in the voltage first, followed by a slower decrease in the voltage (see

also Fig. 3.3). Figs. 3.4a and 3.4b show maxima, and in Fig. 3.4c both a minimum (a_0) and a maximum (b_0) occurs. In table 3.1 the measured dimensions have been compared with ones calculated for a free electron Al Fermi sphere. As only extremal orbits have been observed, the measured maximum (b) should be the same for the three field orientations. The differences in the measured values for b are mainly due to the uncertainty in the measured distance between the point contacts. Better methods to measure this distance in the helium bath or using point contacts fixed on the sample surface would improve these results. However, the measured results are of the same order of magnitude as the calculat-

TABLE 3.1 Comparison of measured and calculated values of extremes in the diameters of orbits on the Fermi surface. $k_F = 1.75 \cdot 10^8 cm^{-1}$, the momentum of free electrons at the Fermi energy for aluminium; a and b give the minimal and maximal extreme of the orbit respectively.

B //	a/k_F		b/k_F	
	meas.	calc.	meas.	calc.
$[01\bar{1}]$	-	-	0.76	0.71
$[11\bar{1}]$	-	-	0.68	0.71
$[21\bar{1}]$	0.49	0.57	0.69	0.71

ed ones. In Fig. 3.4c perhaps focusing of electrons that have been reflected specularly from the crystal surface (a_1), can be seen. The hilly crystal surface or the always present oxide layer might be the cause of the weakness of these voltage peaks. However, from many similar observations on different places on the sample surface we estimate the coefficient for specular reflection for this surface to be 0.3. Better polishing techniques might cause a higher coefficient for specular reflection.

At temperatures lower than 2 Kelvin anomalies in the collector voltage, dependent on the temperature and the magnetic field strength, were observed. Fig. 3.5 shows measured collector voltages as a function of

applied magnetic field at different temperatures. At particular field strengths spikes in the voltage are visible, increasing with decreasing

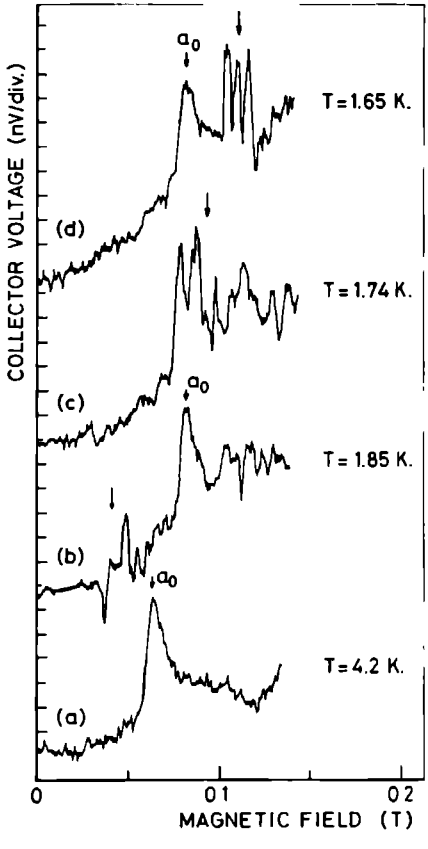

Fig. 3.5
Experimental results at different temperatures showing temperature and magnetic field dependent disturbances of the collector voltage, denoted by the large arrow. The signal a_0 is the direct electron focusing peak.

temperatures. The phenomenon itself was rather reproducible, however, the exact shape of these anomalies were not. The cause of the anomaly could be that part of the metal below the collector becomes superconducting, far above the critical temperature for superconductivity of Al (1.18 K). Spotwelding the tungsten point contacts on the crystal surface is most likely the reason for it. As both the tungsten wire and the aluminium crystal surface were covered with an oxide layer, it is very well possible that on spotwelding the crystal is contaminated by oxigen, which increases the critical temperature[8]. Furthermore, because the point contacts had to be spotwelded normally several times to get a

low Ohmic junction, some aluminium could have stuck to the point contacts, resulting in a deformation of the crystal lattice and a disturbance of the electron-phonon coupling in this region. Voltage spikes were registered at the collector when the superconducting parts became normal.

3.4 *Conclusions*

We conclude that we have observed the focusing of electrons in aluminium single crystal on different orbits on the Al Fermi surface. The shape of the focusing signals directly indicates whether local minimal or maximal orbit diameters are measured. However, for more quantitative results on determining extremal diameters of selected orbits on the Al Fermi surface, a better method is necessary to measure the distance between the point contacts in the helium bath. Also focusing of electrons reflected specularly from the crystal surface between the point contacts was observed. For the given crystal surface we found a quite small coefficient for specular reflection (≤ 0.3).

This work is part of the research program of the Stichting voor Fundamenteel Onderzoek der Materie and was made possible by financial support from the Nederlandse Organisatie voor Zuiver Wetenschappelijk Onderzoek.

References

1. V. S. Tsoi, Pis'ma Zh. Eksp. Teor. Fiz. 19, 114 (1974) [JETP Lett. 19, 70 (1974)].
2. V. S. Tsoi, and I. I. Razgonov, Zh. ETF. Pis. Red. 23, 107 (1975) [JETP Lett. 23, 92 (1976)].
3. V. S. Tsoi, and I. I. Razgonov, Pis'ma Zh. Eksp. Teor. Fiz. 25, 30 (1977) [JETP Lett. 25, 26 (1977)].
4. V. S. Tsoi, J. Bass, P. A. M. Benistant, H. van Kempen, E. L. M. Payens and P. Wyder, J. Phys. F: Metal Phys. 9, L221 (1979).
5. N. W. Ashcroft, Phil. Mag. 8, 2055 (1963).
6. Kryal - OZ2, Vereinigte Aluminium Werke, Germany.
7. P. A. M. Benistant, H. van Kempen, and P. Wyder, to be published.
8. R. W. Cohen, and B. Abeles, Phys. Rev. 168, 444 (1968).

ABSTRACT

In this chapter we present a new method to observe Andreev reflection directly, namely, by the magnetic focusing of Andreev-reflected quasiparticles in a normal metal with the use of point contacts. Both double and single point contact techniques are presented. A solution is given for the discrepancies between the experiment and simple Andreev reflection theory. It turns out that the single point contact technique is sufficiently sensitive to observe deviations of the electron paths of the order of 10^{-5} rad. In spite of the fact that the normal-metal-superconductor interface was made under far from ideal circumstances, the experimentally obtained probability for Andreev reflection is found to be 0.7, in very good agreement with 0.7 ± 0.2, the value of a perfect Ag-Pb interface.

If a normal metal is backed by a superconductor, a conduction electron in the normal metal cannot go into the superconductor if its energy is smaller than the gap energy of the superconductor. A. F. Andreev[1] predicted in 1964 that such an electron will be reflected as a hole into the normal metal, adding a Cooper pair to the condensate of the superconductor. This process leads to an extra current flowing into the superconductor, known as excess current. Because of the conservation of momentum, charge, and mass of the system, the signs of the velocity, charge, and mass of the reflected quasiparticle are reversed[2], in contrast to specular reflection, in which only the sign of the velocity component normal to the interface is reversed. This so called Andreev reflection (AR) has been observed in different ways: e.g., by measuring the electric conductivity of a superconductor in the intermediate state[3]; using the radio-frequency size effect[4]; by tunneling measurements[5,6], where the change in the tunneling density of states due to the quantum mechanical interference effects of these different states is measured; by Gantmakher-resonance experiments in the intermediate state[2]; or with the aid of superconducting point contacts[7].

In this paper we report the observation of AR and the focusing of Andreev-reflected particles using normal metal point contacts. We used two experimental set-ups to observe this interesting phenomenon:

1. The double point contact technique.

As has been demonstrated before (e.g. Refs. 8-11), with this technique information can be obtained about the orbits of the charge carriers within a metal single crystal and their reflection from its surface. Two point contacts are placed on a flat surface of a metal single crystal. Electrons are injected into the crystal through one point contact (the emitter) and are deflected by a homogeneous magnetic field, parallel to the surface and perpendicular to the line connecting the point contacts. Either directly or via reflections (e.g. at the crystal surface or other boundaries) they reach the other point contact (the col-

lector). At the collector a magnetic field-dependent voltage is measured, yielding voltage peaks for those electrons injected perpendicular to the crystal surface whether or not reflected from the surface between the point contacts. Bozhko et. al.[12] were able to observe AR through reflection from an evaporated superconducting strip on a normal metal single crystal between the point contacts. In the experiment described in this chapter, however, the electrons were injected at one side of a thin single crystal slab, with a thickness smaller than the mean free path of the electrons, backed at the other side by a superconductor (Fig. 4.1).

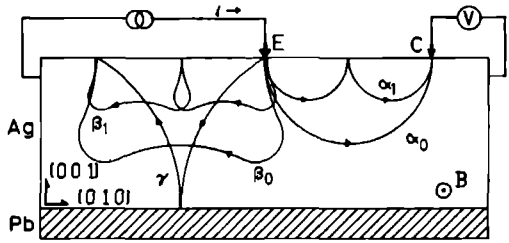

Fig. 4.1 Observation of Andreev reflection using the double point contact technique. Direct focusing of electrons on different orbits on the Ag Fermi surface have been drawn (α_0 and β_0), and focusing after specular reflection from the upper crystal surface (α_1 and β_1). The orbit denoted by γ represents focusing of charged particles after Andreev reflection.

2. The single point contact technique.

With this technique the voltage is measured across the same point contact, through which the current is sent. Also care is taken that the point contact is a good Sharvin junction[13], i.e. the electrons are injected ballistiсly into the crystal. It has been demonstrated by Jansen et. al.[14], that this technique is perfectly suited to study electrons with a particular energy in a metal. Because of the conservation laws described above, in the absence of a magnetic field the Andreev-reflected particles will go back through the same point contact, as

shown in Fig. 4.2. Because the thickness of the slab is much larger than the diameter of the point contact ($\sim 10^4$), this technique offers a very sensitive means to study whether exact retro-reflection, i.e. the reversal of the sign of the quasiparticle velocity on AR, takes place. Furthermore, as the electrons are injected energy-resolved into the crystal, the energy gap of the superconductor can be measured.

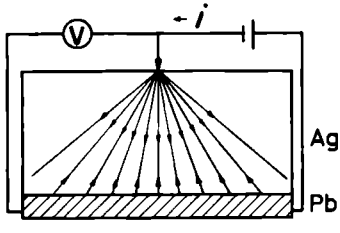

Fig. 4.2
Observation of Andreev reflection using the single point contact technique. In the absence of an external magnetic field, the particles flow back through the same contact.

In the next section the strength of the focusing magnetic field for Andreev-reflected quasiparticles is calculated as a function of the distance between the point contacts and the thickness of the normal metal. Furthermore, an expression is derived for the position where the Andreev-reflected particles reach the upper crystal surface again. Then the two experimental techniques are discussed separately. Finally, in the discussion the results obtained from the two techniques are compared with each other, and a solution is found for the discrepancies between the measured and calculated results.

4.2 *Magnetic focusing of electrons and holes*

In this section the influence of a uniform magnetic field on the Andreev reflection process is discussed using the free electron approximation. An expression is found for the place where the quasiparticles reach the upper crystal surface again after Andreev reflection.

4.2.1 *The normal-metal-superconductor interface*

Consider a conduction electron in a normal metal approaching a normal-metal-superconductor (N-S) interface. If the electron energy is larger than the gap energy of the superconductor, the electron can be transmitted into the superconductor as a quasiparticle. However, if the quasiparticle energy is smaller than the gap energy, it cannot be transmitted, leaving only the possibility for specular or Andreev reflection, depending on the quality of the interface. To handle the interface we start from the Bogoliubov equations[15], given by

$$i\hbar\frac{\partial f}{\partial t} = \left[-\frac{\hbar^2\nabla^2}{2m} - \mu(x) + V(x)\right]f(x,t) + \Delta(x)g(x,t) \qquad (4.1a)$$

$$i\hbar\frac{\partial g}{\partial t} = -\left[-\frac{\hbar^2\nabla^2}{2m} - \mu(x) + V(x)\right]g(x,t) + \Delta(x)f(x,t) \qquad (4.1b)$$

where $\Delta(x)$ is the energy gap and $\mu(x)$ the chemical potential. In the normal metal $[\Delta(x) = 0]$, Eq. (4.1a) is the Schrodinger equation for electrons, while Eq. (4.1b) is the time-reversed Schrodinger equation for electrons. Since an electron satisfying the time-reversed Schrodinger equation behaves in many ways like a hole, $g(x,t)$ is called the hole wave function. As can be seen from Eq. (4.1) the electron and hole wave functions are not coupled for a normal metal. However, in a superconductor ($\Delta \neq 0$) the wave functions do couple together and one can no longer speak about pure electronlike or holelike quasiparticles in a superconductor. In this experiment we are concerned about what happens with quasiparticles in a normal metal before and after AR, so we do not go into further detail about what happens in the superconductor itself. Starting from the Bogoliubov equations, Blonder et. al.[16] derived the probablity for a quasiparticle to reflect or transmit from an N-S interface. Our experiment had been set up in such a way that apart from electron focusing (EF), i.e. focusing of electrons on orbits denoted by α and β in Fig. 4.1, only focusing of quasiparticles after Andreev reflection (AR) could be observed, on the orbit denoted by γ in Fig. 4.1. Therefore, we will concern ourselves only with the probability for AR,

A, at an N-S interface. According to Blonder et. al. we have the following expression

$$A = [\varepsilon'^2 + (1 - \varepsilon'^2)(1 + 2Z^2)^2]^{-1} \qquad \varepsilon' < 1 \qquad (4.2a)$$

$$A = [\varepsilon' + (\varepsilon'^2 - 1)^{1/2}(1 + 2Z^2)]^{-2} \qquad \varepsilon' > 1 \qquad (4.2b)$$

where $\varepsilon' = \varepsilon/\Delta$, the ratio of the quasiparticle energy to the gap energy of the superconductor; Z is defined as a dimensionless measure of the barrier located at the interface. This barrier can consist of a repulsive potential[16], $V = H\delta(x)$, but a difference in the Fermi velocities of the two metals will also result in some normal reflection. This leads to the following expression for Z[7]:

$$Z = [(k_F H/2\varepsilon_F)^2 + (1 - \underline{r}^2)/4\underline{r}]^{1/2} \qquad (4.3)$$

with $\underline{r}$ the ratio of the Fermi velocities of the two metals. It follows from Eq. (4.2) that for $\varepsilon = \Delta$, $A = 1$ for any value of Z. At lower energies $A < 1$ for $Z > 0$ (Fig. 4.3). Notice, that if the Fermi velocities

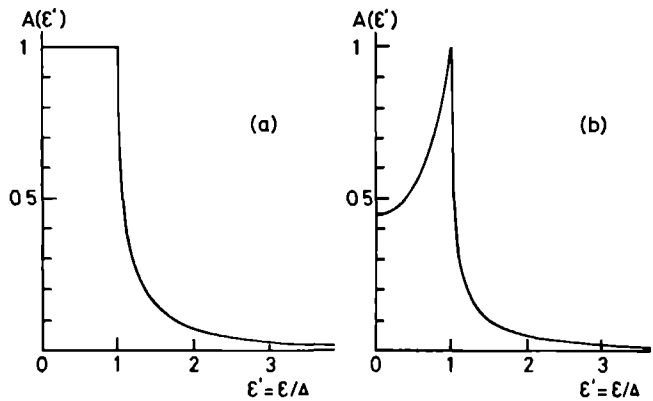

Fig. 4.3 Plot of Eq. (4.2) for an ideal (Z = 0) N-S interface (a) and for an N-S interface with a potential barrier (b) (Z = 0.5). Notice, that A=1 at the gap energy Δ of the superconductor independent of the barrier height.

are different, even for an ideal N-S interface the AR probability is less than one at zero excitation energy. Below the energy gap the probability for specular reflection from the N-S interface, $B = 1 - A$, as the transmission probability is zero in this case. A detailed derivation of the reflection and transmission probabilities above the gap has been given in Ref. 16.

Fig. 4.4 shows a simplified picture of AR in one dimension. The electron excitation branch is plotted as the solid line, and the hole

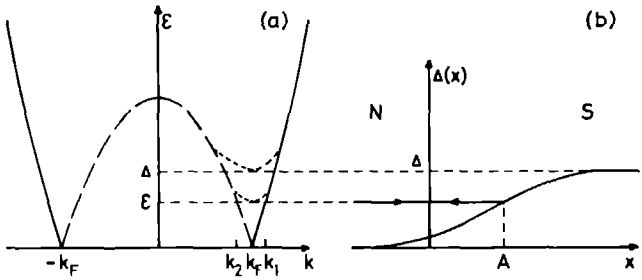

Fig. 4.4 AR in one dimension. A quasiparticle in the electron excitation branch with momentum k_1 approaches the superconductor. Near the N-S interface the energy gap $\Delta(x)$ starts to build up. If $\Delta(x)$ equals the quasiparticle energy, the quasiparticle is reflected back into the normal metal, however, now being in the hole branch with momentum $k_2 \sim k_1$.

branch as the dashed line. Suppose that the incoming quasiparticle is electronlike, having an energy ε_1, and a momentum $|\vec{k}_1| = k_F + \delta k$, moving with a velocity $\vec{v}(\vec{k}_1) = \partial\varepsilon/\partial\hbar\vec{k}$ in the direction of $\vec{k}_1$. Near the interface the gap starts to build up and at a certain place, denoted by A, the gap energy equals the quasiparticle energy. Because of conservation of momentum interband transition takes place, leaving the excitation with momentum $|\vec{k}_2| = k_F - \delta k$. However, now its group velocity is opposite to $\vec{k}_2$. As, from a classical point of view, $\vec{v} = \vec{p}/m = \hbar\vec{k}/m$, we may speak of a negative mass of these holelike excitations. Concluding, we can say that on AR the sign of momentum is conserved ($\delta k \ll k_F$), while the signs of velocity, charge, and mass are reversed.

It is well known that there is no difference in the currents carried by electrons moving in one direction and holes moving in the opposite direction. However, in this section it will be shown that in a homogeneous magnetic field the motion of a hole is not the time reversal of the motion of an electron with the opposite incident velocity.

The semiclassical equations of motion for a particle with a charge q and a velocity $\vec{v}(\vec{k})$ in a homogeneous magnetic field $\vec{B}$ are given by

$$\vec{v}(\vec{k}) = \frac{1}{\hbar} \frac{\partial \varepsilon(\vec{k})}{\partial \vec{k}} \tag{4.4}$$

$$\hbar \dot{\vec{k}} = q\, \vec{v}(\vec{k}) \times \vec{B} \tag{4.5}$$

Fig. 4.5 illustrates the AR process in k-space and in real space in the semiclassical picture. Initially the momentum of the electron system equals $\vec{k}_1$ (Fig. 4.5a). At the N-S interface the incoming electron forms a Cooper pair with the electron with (almost) opposite momentum but with the same energy with respect to the Fermi energy. The Cooper pair disappears into the superconductor. The signs of the velocity, $\sim \partial\varepsilon/\partial\vec{k}$ [Eq. (4.4)], and the charge of the remaining hole are opposite to those of the original electron, so $\dot{\vec{k}}$ is conserved [Eq. (4.5)], and the hole continues to rotate in the same direction in k-space as the electron (Fig. 4.5b). The momentum of the electron opposite to the remaining hole is not compensated any more, and the momentum of the system becomes $\vec{k}_2$, about the same as the momentum of the incoming electron, but opposite to the velocity of the hole. For free electrons $\varepsilon(\vec{k}) = \hbar^2 k^2/2m$, and therefore $\vec{v}(\vec{k}) = \hbar\vec{k}/m$. The acceleration of the particle is then given by

$$\vec{a}(\vec{k}) = \frac{d\vec{v}}{dt} = \frac{\hbar\dot{\vec{k}}}{m} \tag{4.6}$$

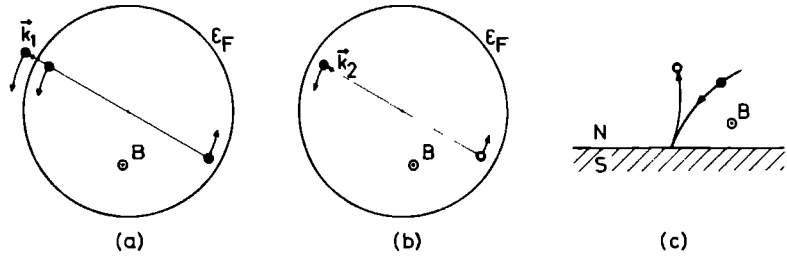

Fig. 4.5 Semiclassical picture of the AR process at an N-S interface in a uniform magnetic field; (a) Fermi sphere with one electron added to the electron system, having momentum $\vec{k}_1$; (b) at the N-S interface this electron forms a Cooper pair with an electron with opposite momentum, leaving the electron system with momentum $\vec{k}_2 = \vec{k}_1$; (c) the AR process in real space, although the sign of the velocity is reversed on AR, the orbit of the outcoming hole is not the time reversal of the orbit of the incoming electron.

As $\vec{v}$ is opposite to $\vec{k}$, we can speak of a negative mass, and the sign of the acceleration of the hole is opposite to that of the incoming electron. It means that in real space the Andreev-reflected particle does not move back over the same orbit as the incoming electron (Fig. 4.5c). Therefore, it is possible to observe AR with two point contacts.

4.2.3 *Focusing of charged particles after Andreev reflection*

For a charged particle injected at the origin into a normal metal single crystal slab of thickness D, we define polar angles ϕ and α in such a way that

$$\vec{v}(0) = v_F(-\sin\alpha\sin\phi, \cos\phi, -\cos\alpha\sin\phi) \qquad (-\tfrac{\pi}{2} < \alpha < \tfrac{\pi}{2},\ 0 < \phi < \pi) \qquad (4.7)$$

is the velocity of the incoming particle supposing that it has the Fermi energy (Fig. 4.6). A homogeneous magnetic field directed along the positive y-axis, deflects the particle and after a time t the particle

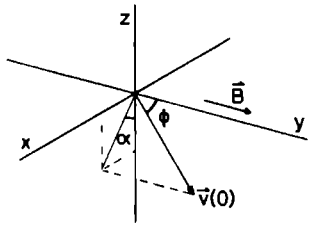

Fig. 4.6
Definition of α and φ. The upper crystal surface lies in th xy-plane; the emitter is located at the origin.

velocity and position are

$$\vec{v}(t) = v_F \left[\sin(\frac{qBt}{m} - \alpha)\sin\phi, \cos\phi, -\cos(\frac{qBt}{m} - \alpha)\sin\phi\right] \tag{4.8}$$

$$\vec{r}(t) = \frac{mv_F}{qB}\left[-(\cos(\frac{qBt}{m} - \alpha) - \cos\alpha)\sin\phi, \frac{qBt}{m}\cos\phi,\right.$$

$$\left. -(\sin(\frac{qBt}{m} - \alpha) + \sin\alpha)\sin\phi\right] \tag{4.9}$$

If the sample thickness is larger than twice the cyclotron radius of the particle orbit, the particle cannot reach the bottom side of the slab. After a time T_o, however, it reaches the upper surface again. The condition $r_z(T_o) = 0$ yields

$$T_o = m(\pi + 2\alpha)/qB \tag{4.10}$$

leading to a particle position at the surface

$$\vec{r}(T_o) = \frac{mv_F}{qB}\left[2\cos\alpha\sin\phi, (\pi + 2\alpha)\cos\phi, 0\right] \tag{4.11}$$

The condition for normal electron focusing[11] (EF) is achieved when $\alpha = 0$. As long as the cyclotron radius is larger than the sample thickness, there are angles of incidence for which the particle can reach the bottom side of the slab. The time the particle needs to reach the bottom is found from the condition $r_z(T_1) = -D$. This gives

$$T_1 = \frac{m}{qB}\left[\alpha + \arcsin(\frac{qBD}{mv_F\sin\phi} - \sin\alpha)\right] \tag{4.12}$$

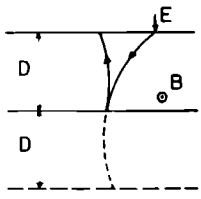

Fig. 4.7
From geometrical arguments it is easy to see that the time needed for the particle after AR at (x,y,-D) to reach the upper crystal surface, is equal to the time an unperturbed particle would need to arrive at (x',y',-2D).

After AR the particle can reach the upper surface again at a time T_2. From symmetry arguments it can be seen that T_2 is given by the condition $r_z(T_2) = -2D$, if the particle would have followed its original path (Fig. 4.7). This yields

$$T_2 = \frac{m}{qB}\left[\alpha + \arcsin\left(\frac{2qBD}{mv_F\sin\phi} - \sin\alpha\right)\right] \tag{4.13}$$

The place were the quasiparticle reaches the crystal surface after AR is now given by $\vec{r}^{AR}(T_2) = \vec{r}(T_1) - \left[\vec{r}(T_2) - \vec{r}(T_1)\right]$. This yields

$$r_x^{AR}(T_2) = -\frac{mv_F\sin\phi}{qB}\left\{2\left[1 - \left(\frac{qBD}{mv_F\sin\phi} - \sin\alpha\right)^2\right]^{1/2} - \left[1 - \left(\frac{2qBD}{mv_F\sin\phi} - \sin\alpha\right)^2\right]^{1/2} - \cos\alpha\right\} \tag{4.14a}$$

$$r_y^{AR}(T_2) = (2T_1 - T_2)\, v_F\cos\phi \tag{4.14b}$$

$$r_z^{AR}(T_2) = 0 \tag{4.14c}$$

In the following the superscript AR in Eq. (4.14) is omitted.

It can be shown that, if the time for the incoming particle to go from the emitter to the N-S interface is equal to the time the Andreev-reflected particle needs to reach the upper surface again, i. e. $T_2 = 2T_1$, $r_x(T_2)$ takes on a minimal value and $r_y(T_2) = 0$. Because the absolute value of the quasiparticle velocity is the same before and after AR, the length of the orbit from the upper surface to the N-S interface must be equal to the length of the orbit from the N-S interface

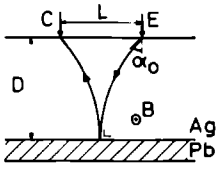

Fig. 4.8
If the angle of incidence at the emitter is such that the electron is normally incident on the N-S interface, both r_x is minimal and focusing takes place at the upper crystal surface.

back to the upper surface. This is the case if the particle is normally incident to the interface (Fig. 4.8). The condition $T_2 = 2\pi_1$ is satisfied if the angle of incidence at the emitter $\alpha = \alpha_o$, given by

$$\alpha_o = \arcsin\left(\frac{qBD}{mv_F \sin\phi}\right) \tag{4.15}$$

It is easy to show that $\partial r_x/\partial\alpha = 0$ for $\alpha = \alpha_o$, giving the focusing condition. This means that in contrast to EF, focusing now does not occur when the particles are injected normal to the crystal surface at the emitter, but when they are normally incident to the N-S interface. Now $r_x(T_2, \alpha_o)$ becomes

$$r_x(T_2, \alpha_o) = -\frac{2mv_F \sin\phi}{qB}\left\{1 - \left[1 - \left(\frac{qBD}{mv_F \sin\phi}\right)^2\right]^{1/2}\right\} \tag{4.16}$$

Notice, that for EF we have $r_x = (2mv_F \sin\phi)/qB$ for the focusing condition $\alpha = 0$ [Eq.(4.11)]. Because $r_y(T_2, \alpha_o)$ equals zero, particles injected into the normal metal at the emitter with a velocity component parallel to the applied magnetic field, are also deflected back to the x-axis, contrary to EF. Consequently, the solid angle in which electrons have to enter the crystal at the emitter in order to be focused on the collector, is, for a sample thickness of 200 μm, about 15 times larger for AR than for EF, according to computer simulations. Fig. 4.9 shows a computer plot in three dimensions of the distribution of the number of particles arriving at the crystal surface after AR.

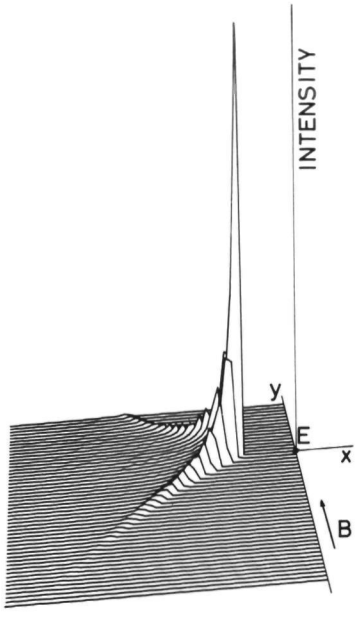

Fig. 4.9
Computer plot of the number of Andreev-reflected particles per unit area in the upper crystal surface. Notice, that the highest particle density is on the line through the emitter perpendicular to the direction of the applied magnetic field.

4.3 *Experimental results*

In this paragraph we present experimental results in which the focusing of Andreev-reflected particles is observed. First the results obtained with the double point contact technique are given, followed by those obtained with the single point contact technique.

Although it seems that the two techniques differ only by one point contact, in reality there were more experimental differences. Firstly, in the double point contact technique tungsten wires were used for the point contacts and the measurements were performed with low Ohmic spotwelded contacts ($\sim 0.1\ \Omega$). On the contrary, the single point contact technique measurements were performed with an Ag-Ag contact with a higher resistance ($\sim 2\ \Omega$) to obtain information about the energy dependence of the AR process. Secondly, in the former technique an emitter current of 300 mA could be used, whereas in the latter one the current was only 0.1 mA. Thirdly, the strength of the applied magnetic field

was of the order of 0.1 T in the first technique compared with $\sim 10^{-5}$ T in the second one.
However, both techniques have in common that the same AR process is observed, and that the measurements were done on the same sample.

4.3.1 *Sample preparation*

To observe the focusing of the Andreev-reflected particles an Ag single crystal slab was used with a Pb layer fixed on one side. Pb has a superconducting critical temperature[17] of 7.2 K and a critical field at 0 K of 0.0803 T. So at 4.2 K the critical field is already of the same order of magnitude as the expected focusing field strengths ($\sim 10^{-2}$ T). Furthermore, the coherence length or the depth the quasiparticles penetrate into the superconductor (see Fig. 4.4), is for Pb only 800 Å. Finally, Ag and Pb are immiscible[18].

The Ag slab was spark-cut from a 99.9999 % pure single crystal rod[19]. It was polished with mechanical techniques using diamond pastes with grains down to 6 μm (Struers) and an alumina polishing suspension (Baikalox), and etched chemically in a 20 ml NH_3 solution (> 25%) with 6 drops of a 40% H_2O_2 solution added[10]. Thus a thickness of about 200 μm was obtained. To release mechanical stresses and increase the residual resistance ratio [RRR = R(300 K)/R(4.2 K)], the sample was annealed for 16 hours at 800 °C at a pressure of 10^{-3} Torr of air[20]. For the single crystal rod, annealed in the same manner, a RRR of 15000 was found, corresponding to an electron mean free path of about 700 μm at low temperatures, much larger than the sample thickness. Before the deposition of Pb the sample was sputter cleaned in a glow discharge of N_2 for about 20 min at a pressure of 10^{-1} Torr. Finally, a layer of 1.5 μm 99.9995 % pure Pb (Balzers) was evaporated on one side of the Ag slab (held at 50 °C) at a pressure of 10^{-6} Torr.

As mentioned above, in this case the point contacts were made of 96 μm diameter W wires, etched electrolytically in a 1N KOH solution yielding sharp points of about 1 μm diameter. The contacts were placed on the normal metal side of the sample in the helium bath. The application of a 90 V battery in series with a 1 MΩ resistance across the contacts produced a stable contact of about 0.1 Ω.
The magnetic field was produced by a water-cooled iron-core electromagnet, rotatable through 360° in the horizontal plane. The sample was mounted horizontally in the insert and could be viewed in the helium bath through the unsilvered glass tail of the cryostat. An ac current of about 300 mA was passed through one point contact, the emitter (E), while the voltage across the other contact, the collector (C), was measured using standard lock-in techniques (Fig. 4.10).

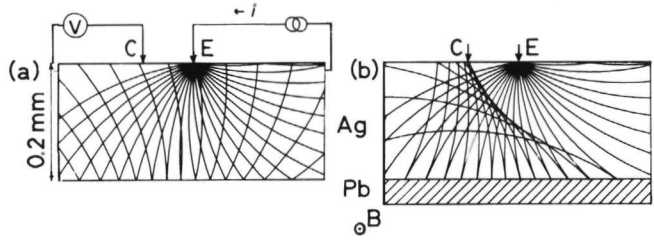

Fig. 4.10 Free electron orbits in a metal in a homogeneous magnetic field. (a) After specular reflection at the bottom of the sample no focusing occurs at the upper surface; (b) Andreev-reflected quasiparticles, however, are focused at the upper surface.

At sufficiently low magnetic field strengths the electrons, injected into the normal metal single crystal slab at the emitter, are able to reach the other side of the slab. Fig. 4.10a shows, that charged particles reflected specularly from this side, won't be focused on the upper side of the slab. Only Andreev-reflected particles can be focused on the collector (Fig. 4.10b), provided that the applied magnetic field has the right direction and strength.

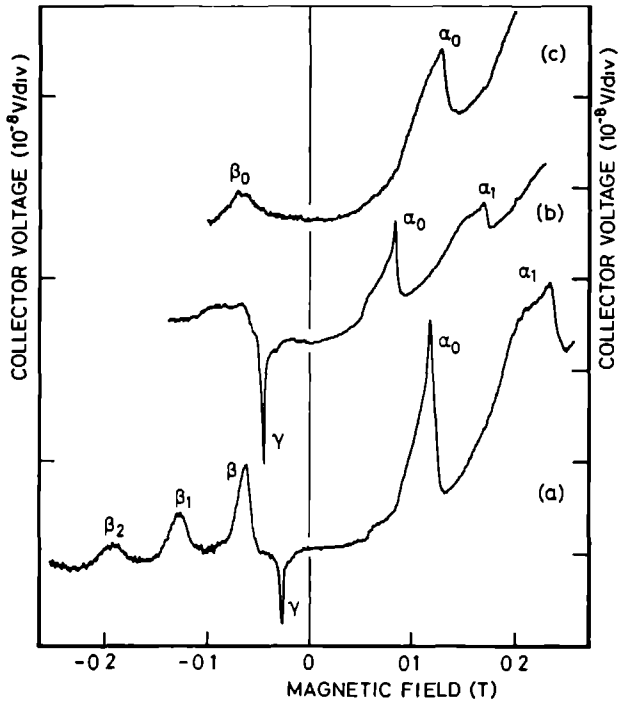

Fig. 4.11 Measured collector voltage as a function of applied magnetic field at 4.2 K (a,b), and above 7.2 K (c). Focusing of different types of orbits can be seen: "electron" (belly) orbits, focused directly (α_0) or via reflection from the upper crystal surface (α_1); "hole" (four-cornered-rosette) orbit (β_0,β_1); Andreev-reflected particles on belly orbits (γ), observed only below 7.2 K. (a) and (b) are measurements for different distances between the point contacts. Note the different voltage scales for the right- and lefthand part of the figure.

Fig. 4.11 shows measured collector voltages as a function of applied magnetic field. The field is oriented along the [100] axis of the Ag crystal. Figs. 4.11a,b show measurements at 4.2 K, for two different distances between the point contacts, while Fig. 4.11c has been recorded above 7.2 K, the critical temperature of Pb. The signals α and β are caused by focusing of electrons on different orbits of the Ag fermi surface: i. e. electronlike (belly) orbits and holelike (four cornered

rosette) orbits respectively (cf. the orbits α and β in Fig. 4.1). The subscript denotes the number of times the electrons have been reflected specularly from the upper Ag surface between the emitter and the collector. The coefficient for specular reflection for this Ag surface, the ratio of α_1 and α_0 (or β_1 and β_0), has been estimated to be[11] 0.8 + 0.1. As both sides of the Ag slab have been prepared in the same way before the deposition of the Pb layer, we expect that the coefficient for specular reflection at the N-S interface will also be in the same order of magnitude. That is, the crystal surface at the bottom is rather flat on atomic scale. The signals α and β shown in Fig. 4.11c are smaller than those shown in Fig. 4.11a,b because at 7.2 K the electron-phonon interaction has increased already considerably compared with the interaction at 4.2 K. Finally, the signals denoted by γ are caused by the focusing of Andreev-reflected quasiparticles on belly orbits (cf. the orbit γ in Fig. 4.1).

That the signals γ are indeed due to AR is supported by the following experimental observations:

1. The absence of the signal above the superconducting critical temperature of Pb. The construction displayed in Fig. 4.10a shows that in the absence of a superconductor at the bottom of the sample no focusing of charged particles reflected specularly from this side can take place at the collector.

2. The sign of the signal. As Figs. 4.11a,b show, the signals γ have a sign opposite to that of the signals α and β. This is in agreement with AR where the sign of the charge of the quasiparticles is inverted on reflection.

3. The orientation of the applied magnetic field. Fig. 4.1 shows that if the field orientation is kept the same, the quasiparticles on belly orbits (α) arrive at the upper crystal surface on the opposite side from the emitter from the quasiparticles on the same orbits that have been Andreev-reflected from the bottom side of the crystal (γ). This is in agreement with our measurements (Figs. 4.11a,b), where the signals α occur at opposite magnetic field orientation from the signals γ.

4. The strength of the focusing field as a function of the distance between the point contacts. Fig. 4.12 compares what happens when the applied magnetic field is increased for EF and AR: for EF the pattern

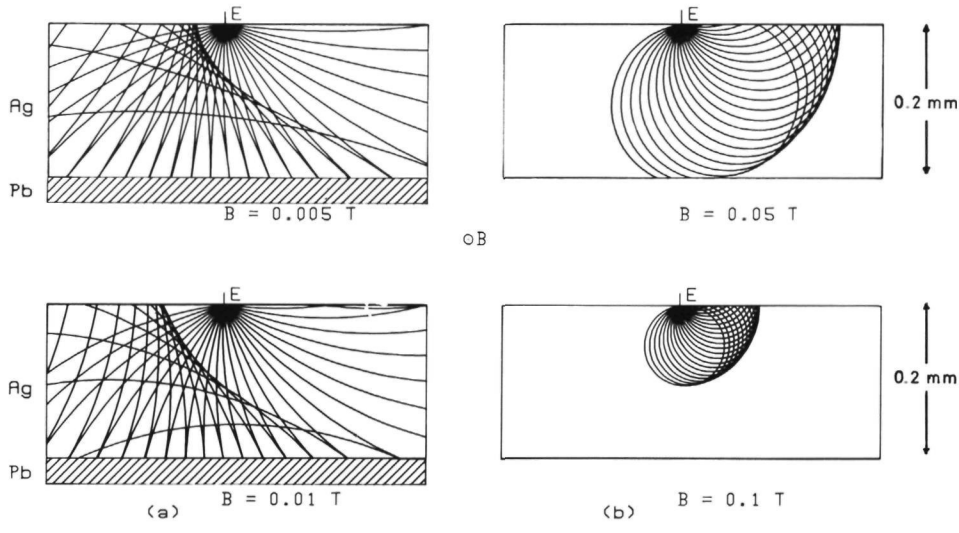

Fig. 4.12 When the applied magnetic field is increased, Andreev-reflected particles are focused further away from the emitter (a), while directly focused particles reach the surface closer to the emitter (b).

moves towards the emitter, while for AR it moves away from the emitter. This is also in agreement with the experimental results as can be seen when comparing Fig. 4.11a with 4.11b. The signal α_o moves to a lower field strength, the signal γ, however, moves to a higher strength. This behaviour can be explained more quantitatively as follows. From Eq. (4.11) it can be seen that the relation between the focusing field strength B_o^{EF} and the distance between the point contacts L, if the field is directed perpendicular to the line connecting the contacts [$\phi = \pi/2$, $L = r_x(T_o)$], is given by

$$B_o^{EF} = 2mv_F/qL \tag{4.17}$$

From Eq. (4.16) a relation can be derived between L, the thickness D of the normal metal, and the strength of the focusing field B_o^{AR} in the case of AR:

$$B_o^{AR} = 4mv_F L/[q(L^2 + 4D^2)] \qquad (L \leq 2D) \qquad (4.18)$$

Combining these two equations we find the relation between the focusing fields:

$$B_o^{AR} = 2B_o^{EF}/[1 + (qDB_o^{EF}/mv_F)^2] \qquad (4.19)$$

In Fig. 4.13 this relation has been plotted for different values of the sample thickness D as the solid lines. Measured results are given by the dots. From these measurements the mean thickness of the normal metal was estimated to be D = 180 ± 14 μm.

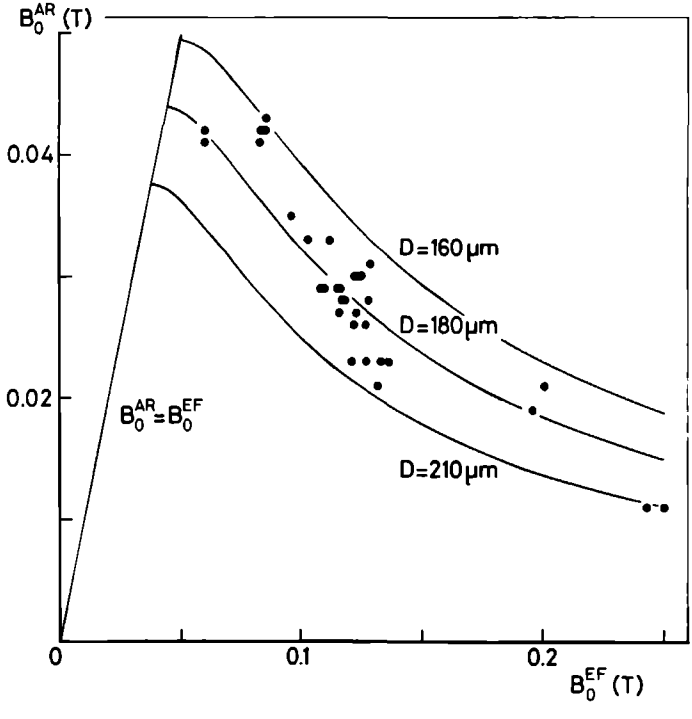

Fig. 4.13 The relation between B_o^{AR} and B_o^{EF} plotted for different crystal thicknesses, D, as the solid lines. The experimental results have been indicated by dots. The curve $B_o^{AR} = B_o^{EF}$ gives the maximal field strength at which AR can be observed (see text).

If the distance L between the point contacts equals 2D, Eq. (4.18) becomes $B_o^{AR} = 4mv_F L/(2qL^2) = 2mv_F/qL = B_o^{EF}$. It is clear from Eq. (4.15) that in this case the focusing angle of incidence at the emitter, $\alpha_o = \pi/2$. When the distance between the point contacts is larger than 2D neither AR nor EF can be observed, as can be seen from Fig. 4.14, where L = 0.46 mm.

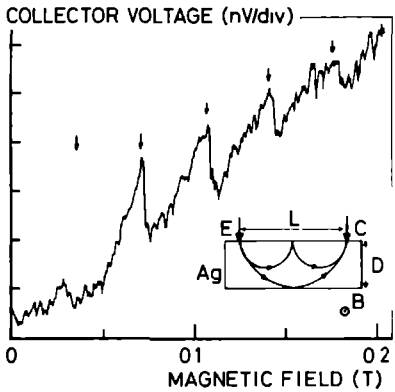

Fig. 4.14
When the distance between the point contacts, L, is larger than twice the sample thickness, D, no direct EF nor AR is possible. Only focusing after one or more specular reflections from the upper crystal surface can be observed.

From the calculated plot in Fig. 4.9 it is clear that the observation of the focusing of Andreev-reflected particles is extremely sensitive to whether the applied magnetic field is oriented perpendicular to the line connecting the point contacts. This is confirmed by the measurements shown in Fig. 4.15, where the intensity of the AR signal and the strength of the focusing field B_o^{AR} has been plotted as a function of the direction of the applied field with respect to the line normal to the line connecting the point contacts. There is a small variation in B_o^{AR} as a function of θ. However, from Fig. 4.9 a decrease in B_o^{AR} might be expected. As the AR pattern moves away from the emitter on increasing field and as the side wings of this pattern also bend away from the emitter, they cross the collector at lower fields than the central peak. We will come back to this later.

It can be shown[11], that electrons injected into the metal single crystal at the emitter, loose their energy immediately, when the injection voltage is larger than about 10 mV. A further proof for this argument is the fact that we were able to observe AR with a voltage across the emitter of about 30 mV, whereas the gap energy of Pb is only 1.4 meV.

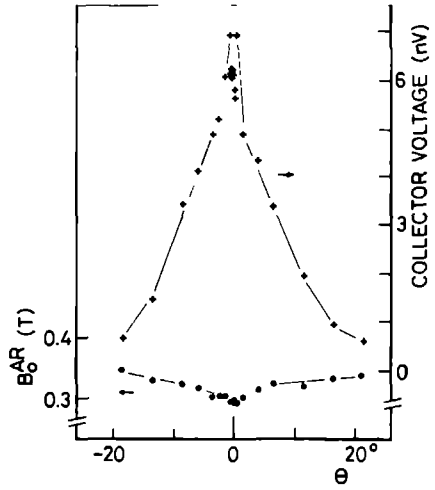

Fig. 4.15
Measured intensity of the AR signal (crosses) and strength of the focusing magnetic field (circles) as a function of the angle, θ, between the direction of the applied magnetic field and the line normal to the line connecting the point contacts (cf. Figs. 4.8 and 4.9).

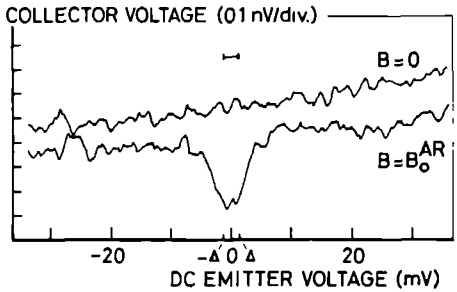

Fig. 4.16 Measured recorder output of the collector voltage as a function of applied dc emitter voltage at B = 0 and B = B_o^{AR} respectively. The modulation voltage across the emitter (1.7 mV peak-to-peak) has been indicated. The recorder pen has not been shifted between the two measurements. Note the finite amplitude of the collector voltage for B = B_o^{AR} at high dc emitter voltages.

Fig. 4.16 shows the measured recorder output of the collector voltage as a function of applied dc voltage across the emitter at zero magnetic field and at the focusing field for AR respectively. The recorder pen has not been shifted between the two measurements. The gap energy Δ of the superconductor and the modulation voltage (1.7 mV peak-to-peak) have been indicated. Although the signal starts to decrease at emitter voltages larger than Δ, AR can still be observed at high dc voltages across the emitter.

We conclude that the magnetic focusing of Andreev-reflected quasiparticles can be studied with the double point contact technique. The expected reversal of the signs of the charge, the mass, and the velocity of the quasiparticles on Andreev reflection has been confirmed.

4.3.3 *The single point contact technique*

In the absence of an external magnetic field the quasiparticles injected into the normal metal at the emitter, will follow straight lines. If AR takes place at the bottom of the metal, they will flow back through the point contact again (Fig. 4.17a), but with reversed character, thus contributing to an extra current, the excess current, through the contact. On the other hand, if only specular or diffuse reflection takes place at the bottom of the sample no focusing occurs at the contact (Fig. 4.17b).

In this experiment the point contact consisted of a 50 μm diameter Ag wire, etched electrolytically in an NaCN solution, to give a point of about 1 μm diameter. Contact was again made in the helium bath, but now by carefully lowering the point onto the normal metal surface without the application of a forming voltage. Thus contact resistances between 1 and 7 Ω were obtained. As has been mentioned above, we assumed that the point contact was a Sharvin junction[13]. In this limit the resistance for a circular contact is given by[14]

$$R_S = \frac{4\rho\ell}{3\pi b^2} \tag{4.20}$$

with ρ the resistivity of the metal. For the sample described here we

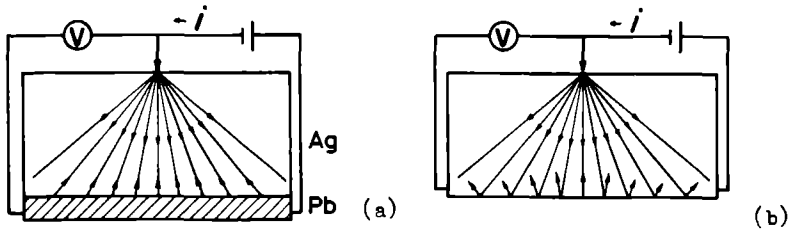

Fig. 4.17 Experimental set up of the single point contact technique. (a) AR at the bottom of the Ag crystal leading to focusing of the Andreev-reflected particles at the point contact; (b) specular reflection does not lead to focusing at the point contact.

calculate a contact radius of 189 Å for a contact resistance of 1 Ω.

From Eq. (4.16) it can be seen that already at very small values of the applied magnetic field r_x may be considerably larger than the point contact dimensions. For example, if B = 10^{-5} T, we find r_x = 506 Å. This means that quasiparticles flowing into the crystal through the point contact are no longer able to flow back through it when the applied field is of the order of 10^{-5} T. Therefore, the insert was placed in a set of two pairs of Helmholtz coils for compensation of the horizontal and vertical components of the earth's field. The measurements were performed at a temperature of 1.2 K to diminish electron-phonon interaction. The resistance R(V) = dV/dI and the voltage derivative of the resistance dR/dV = $(d^2V/dI^2)/(dV/dI)$ were recorded using conventional ac modulation and phase-sensitive detection techniques. The modulation voltage was typically 0.2 mV. In contrast with the double point contact technique the Ag wire had to be etched again after making contact two or three times, because then the point had usually been bent.

Fig. 4.18 shows the measured point contact resistance at zero dc voltage as a function of applied horizontal magnetic field. The vertical field component was kept zero. Notice, that the width of the signal is of the order of the strength of the earth's magnetic field. To observe the energy dependence of AR, the contact resistance as a function of applied dc voltage was measured, shown in Fig. 4.19. For B = 0 (a) the resistance drops when the dc voltage is smaller than Δ/e, while for

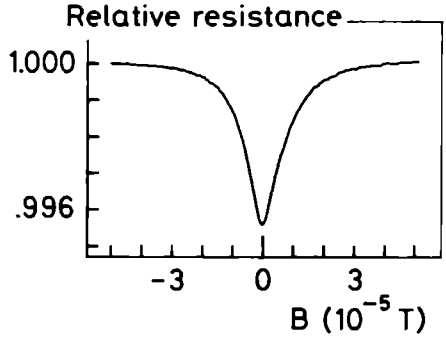

Fig. 4.18
Measured relative resistance of the point contact at zero dc voltage as a function of applied horizontal magnetic field. The vertical field component has been kept zero.

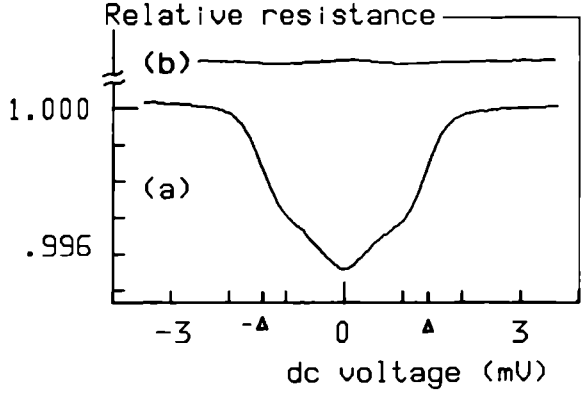

Fig. 4.19 Measured relative resistance of the point contact as a function of applied voltage for B = 0 (a), and B = 5.6•10^{-5} T (b). Notice, that in (b) the resistance stays almost constant as a function of V.

B = 5.6•10^{-5} T (b) the Andreev-reflected particles are deflected from the contact resulting in an almost constant resistance. Subtracting (b) from (a) gives the energy dependence of AR. Although the change in the resistance is only 0.45 %, the signal to noise ratio is much better than in the corresponding measurement with the double point contact technique (cf. Fig. 4.16). Therefore, the single point contact technique is better suited to study the energy dependence of AR.

To check the quality of the point contact, the voltage derivative of the resistance was always measured. In the case of an ideal Sharvin

junction this derivative is equal to the $\alpha^2(\omega)F(\omega)$ function, where $\alpha^2(\omega)$ is an average of the electron-phonon interaction matrix element squared, and $F(\omega)$ the phonon density of states. Fig. 4.20 shows such a measurement for B = 0 (a) and for B = $5.6 \cdot 10^{-5}$ T (b). The structure around

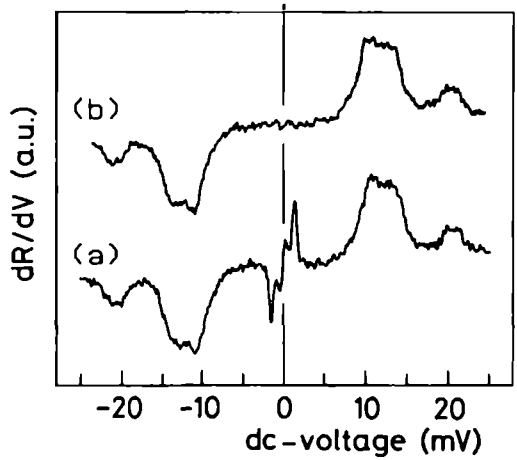

Fig. 4.20 Measured voltage derivative of the point contact resistance as a function of applied voltage for B = 0 (a), and B = $5.6 \cdot 10^{-5}$ T (b). The structure around zero voltage in (a) occurs from AR. These results show that the charge carriers move ballistically through the point contact region.

zero voltage in (a) occurs from AR. Comparison of the results shown in Fig. 4.20 with other experiments[14,21] confirm that the point contact is indeed an ideal Sharvin Ag-Ag junction. So, we can be sure that the electrons are injected into the normal metal ballistically, i.e. without loosing energy at the point contact.

In conclusion we may state that AR and the energy dependence of AR have also been observed with the single point contact technique. In the next section the results obtained from both techniques are compared with each other, and the intensity and width of the signals are explained.

4.4 *Discussion*

So far, we have shown that we are able to observe the magnetic focusing of Andreev-reflected quasiparticles in a normal metal with the use of both the single and double point contact techniques. There remain, however, many interesting questions which can be studied if one performs more quantitative calculations concerning, for example, the quality of the N-S interface and the validity of the Andreev reflection probability as a function of energy [Eq. (4.2)]. There are the following problems:

1. The intensity of the Andreev reflection signal. This intensity should be related more or less directly to the probability for AR at the N-S interface. From this the strength of a possible barrier at the interface can be estimated.
2. The form of the signal as a function of applied magnetic field. For the measurements performed with the single point contact technique it is not difficult to calculate the contact voltage as a function of applied field.
3. The form of the signal as a function of applied dc voltage. These measurements performed with the single point contact technique, should give a direct verification of the energy dependence of AR as given by Eq. (4.2).

4.4.1 *The intensity of the Andreev reflection signal*

In the measurements performed with the double point contact technique, we could assume that the injected electrons all had the Fermi energy. This eliminates one parameter from Eq. (4.2), so that it is possible to make an estimate of the barrier strength at the N-S interface. As has been noted above [Eq. (4.3)], the difference of the Fermi velocities of the two metals reduces also the AR probability, A. Taking for Pb[18]: $v_F = (0.72 \pm 0.06) \cdot 10^6$ m/s, and for Ag[18]: $v_F = (1.07 \pm 0.06) \cdot 10^6$ m/s, we have a ratio $\underline{r} = 1.5 \pm 0.2$. This results in a minimal barrier strength: $Z_{min} = 0.20 \pm 0.06$. Hence, the AR proba-

bility at zero excitation energy is for an ideal N-S interface: $A(0)_{max} = 0.86 \pm 0.08$. Taking, however, for Ag the mean value of the Fermi velocities within 40^{o} from the [001] axis (the directions contributing most to the AR signal) Lengeler et. al.[22] found from de Haas-van Alphen experiments, we find $v_F = (1.49 \pm 0.11) \cdot 10^6$ m/s. This yields $Z_{min} = 0.37 \pm 0.06$ and $A(0)_{max} = 0.6 \pm 0.1$. We therefore estimate the value of the AR probability at zero excitation energy to be $A(0)_{max} = 0.7 \pm 0.2$.

To handle the experimental results, we compare them with the direct EF results, obtained from the same magnetic field sweep. Because, as we have seen before, EF occurs for normally injected electrons, the path length in this case is given by

$$l_p^{EF} = \pi L/2 \tag{4.21}$$

with L the distance between the point contacts. From Fig. 4.8 it can be seen that the path length in the case of AR is given by

$$l_p^{AR} = 2\alpha_o R_c \tag{4.22}$$

where $R_c = mv_F/qB_o^{AR}$, the cyclotron radius of the quasiparticle orbit, and α_o the focusing angle of incidence [Eq. (4.15)]. Substituting Eq. (4.15) and the expression for R_c into Eq. (4.22), we find ($\phi = \pi/2$)

$$l_p^{AR} = \frac{2mv_F}{qB_o^{AR}} \arcsin\left(\frac{qDB_o^{AR}}{mv_F}\right) \tag{4.23}$$

Substituting next Eq. (4.18) into Eq. (4.23) we find the path length as a function of the distance between the point contacts

$$l_p^{AR} = \frac{L^2 + 4D^2}{2L} \arcsin\left(\frac{4LD}{L^2 + 4D^2}\right) \tag{4.24}$$

l_p^{AR} is always larger than l_p^{EF} for the same L, varying from 2D for zero L to l_p^{EF} for maximal L, so this will reduce the AR signal with respect to

EF signal.

Even more drastic is the difference in the angles of incidence for particles contributing to the focusing peaks. For EF this angle is zero, while for the focusing of Andreev-reflected particles it varies from zero to $\pi/2$ depending on L, given by Eq. (4.15). Particles flowing through the contact with an angle α_o, see only a fraction $\cos\alpha_o$ of the contact area. Consequently, the focusing angle of incidence also decreases the AR signal with respect to the EF signal.

However, the solid angle in which the particles have to be injected to contribute to the focusing signal is much larger for AR than for EF, as has been noted above. From computer simulations of the AR signal we found for a sample thickness of 200 µm, a solid angle ratio Ω_{AR}/Ω_{EF} of about 15.

It can be shown[11], that the collector voltage can be written as

$$V_c = I_c R_S = \frac{\Omega}{2\pi} R_S I_e \cos\alpha \, e^{(-l_p/\ell)} \qquad (4.25)$$

where Ω is the solid angle in which electrons have to leave the emitter to contribute to the collector voltage, R_S the collector resistance, and I_e the emitter current. Ω depends on the distance between the point contacts, their area's, and the shape of the Fermi surface. From Eq. (4.25) we can expect the following ratio of the AR signal to the EF signal:

$$\frac{V_{AR}}{V_{EF}} = A \frac{\Omega_{AR}}{\Omega_{EF}} \cos\alpha_o \, e^{\left[-(l_p^{AR} - l_p^{EF})/\ell\right]} \qquad (4.26)$$

with A the probability for AR.

Fig. 4.21a shows the ratios of measured and calculated AR to EF intensities as a function of the distance between the point contacts, while Fig. 4.21b displays the probability for AR, calculated from the results of Fig. 4.21a. Notice, that all measured ratios are smaller than the calculated ones, and that the probability for AR seems to depend on the distance between the point contacts. Although the quality of the N-S interface was not the same everywhere, this should not be a

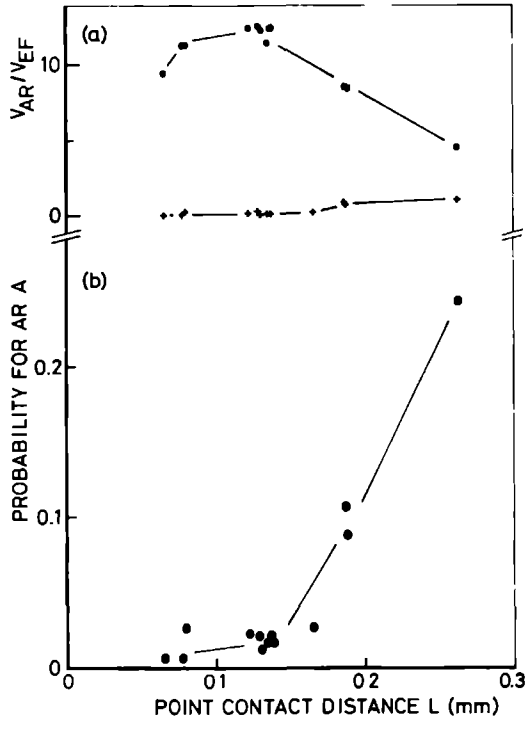

Fig. 4.21 Attempt to estimate the probability for AR, A, from the double point contact measurements. (a) Measured (crosses) and calculated (circles) ratios of the AR signal to the EF signal as a function of the distance between the point contacts, L; (b) calculation of A using Eq. (4.26); A seems to be dependent on L.

reason for an L dependence of A, for the measurements were performed on arbitrary places on the crystal surface. We will come back to this later.

Also the expected relative point contact resistance can be calculated for the results obtained with the single point contact technique. Only those particles that traverse the normal metal without scattering, will flow back through the point contact after AR, thus contributing to the excess current. Therefore, the total current through the point contact is given by

$$I = \int d\Omega \frac{1}{\pi} I_o \cos\theta \left[1 + A\, e^{(-l_p/\ell)}\right] \qquad (4.27)$$

with I_o the applied current through the point contact, and θ the angle of incidence of the incoming electron contributing $(I_o/\pi)\cos\theta$ to the current. Notice, that if the electron mean free path, ℓ, is infinite and the AR probability, A = 1, the total current is obviously twice the applied current. The total path length of the quasiparticle, l_p, equals $2D/\cos\theta$, with D the thickness of the Ag crystal. At low voltages (V < 2 mV), in the absence of AR, we may assume an Ohmic behaviour of the point contact, as can be seen from Fig. 4.20b. So we can write: $R = V/I_o \simeq R_S$, the measured Sharvin resistance in the absence of AR at zero dc voltage. If Andreev-reflected particles are focused on the point contact, the resistance becomes

$$R = R_S \cdot I_o/I = R_S/\left[1 + 2A \int_0^1 d\cos\theta\, \cos\theta\, e^{(-2D/\ell\cos\theta)}\right] \qquad (4.28)$$

Taking ℓ = 700 μm, D = 200 μm, and $A = A(0)_{max} = 0.7$, we find $R/R_S = 0.80$, much larger than the measured value of 0.0045. From this and from the results obtained with the double point contact technique for small point contact distances, it would follow that $A \sim 0.01$.

We can conclude that this interpretation of the experiment, which assumes an ideal retro-reflection but non-ideal AR probability, leads to results that are inconsistent, namely, a large difference between the measured and calculated signal intensities, and an AR probability that varies depending on the distance between the point contacts. As will be shown in the next section, there are even stronger arguments to abandon the used assumptions and replace them with a completely different model.

4.4.2 *Andreev reflection as a function of applied magnetic field*

Especially for the single point contact technique the form of the AR signal as a function of applied magnetic field can be easily calculated. In the previous section it has been shown that at zero field all injected quasiparticles return, if they have been Andreev-reflected, through the same contact, yielding a relative resistance drop of 20 % for ideal AR, and for the given sample thickness and electron mean free path.

As the magnetic field strengths are very small ($\sim 10^{-5}$ T), the place where the Andreev-reflected quasiparticle reaches the crystal surface can be approximated by

$$r_x = \frac{qBD^2}{\hbar k_F \cos\theta} (\tan^2\theta\cos^2\phi + 1) \qquad (4.29a)$$

$$r_y = \frac{qBD^2}{\hbar k_F \cos\theta} \tan^2\theta\sin\phi\cos\phi \qquad (4.29b)$$

with B oriented along the positive y-axis, and θ and ϕ polar angles with the pole now normal to the crystal surface, in contrast to Eq. (4.14), where the pole was along the field direction. A particle injected through the point contact at position $\vec{r}_o$ reaches the crystal surface after AR at $\vec{r}_o + [r_x(\theta,\phi), r_y(\theta,\phi), 0]$. So, for a given set of θ and ϕ the point contact area will be represented on the surface by a spot with the same area at a distance d(B), given by

$$d(B) = [r_x^2(\theta,\phi) + r_y^2(\theta,\phi)]^{1/2} = \frac{qBD^2}{\hbar k_F \cos^3\theta} [1 + \sin^2\phi(\cos^4\theta - 1)]^{1/2} \qquad (4.30)$$

The fraction of particles flowing back through the point contact for a given angle of incidence, is simply the ratio of the overlap of the two areas to the point contact area, F(B), given by

$$F(B) = (2/\pi)\arccos(d/2b) - (d/\pi b)(1-d^2/4b^2)^{1/2} \qquad (d<2b) \quad (4.31)$$

with b the radius of the point contact. Integration over θ and ϕ yields the relative resistance as a function of applied magnetic field:

$$R(B) = R_S/\left[1 + \frac{A}{\pi}\int_0^{2\pi} d\phi \int_0^1 d\cos\theta \cos\theta\, F(B)\, e^{(-2D/\ell\cos\theta)}\right] \qquad (4.32)$$

where F(B) is given by Eq. (4.31). Because F(0) = 1 for any θ and ϕ, Eq. (4.32) reduces to Eq. (4.28) for B = 0. The maximal width of the signal is given by the maximal magnetic field for which a quasiparticle starting from one side of the point contact, can flow back through the contact at the other side i.e. $d_{min}(B_{max}) = 2b$. In the low field approximation d(B) takes on a minimal value for $\theta = 0$, and the maximal field strength is given by

$$B_{max} = 2b\hbar k_F/qD^2 \qquad (4.33)$$

Fig. 4.22 shows a plot of Eq. (4.32) as the dotted curve together with the measured result (solid curve); the calculated curve is normalized to the measured one at B = 0. The measured Sharvin resistance was 2.14 Ω, yielding a contact radius, b = 126 Å [Eq. (4.20)], and a maximal magnetic field, $B_{max} = 5.0 \cdot 10^{-6}$ T. Notice, that apart from the great difference in intensity (~ 45), the measured signal is much broader than the calculated one, and therefore broader than is possible for ideal retro-reflection.

It would be interesting to know how many quasiparticles actually have been Andreev-reflected. A first approximation is to assume that the measured signal as a function of applied magnetic field equals the pattern of Andreev-reflected quasiparticles at the crystal surface at zero field, and neglect the deformation of this pattern caused by the magnetic field (Fig. 4.9). It turns out that the integral of $2\pi B \cdot R(B)$ is approximately the same for the measured result and for the calculated result with ideal retro-reflection and an AR probability equal to one. This indicates that almost all incoming quasiparticles are Andreev-reflected at the N-S interface, but that they are not retro-reflected

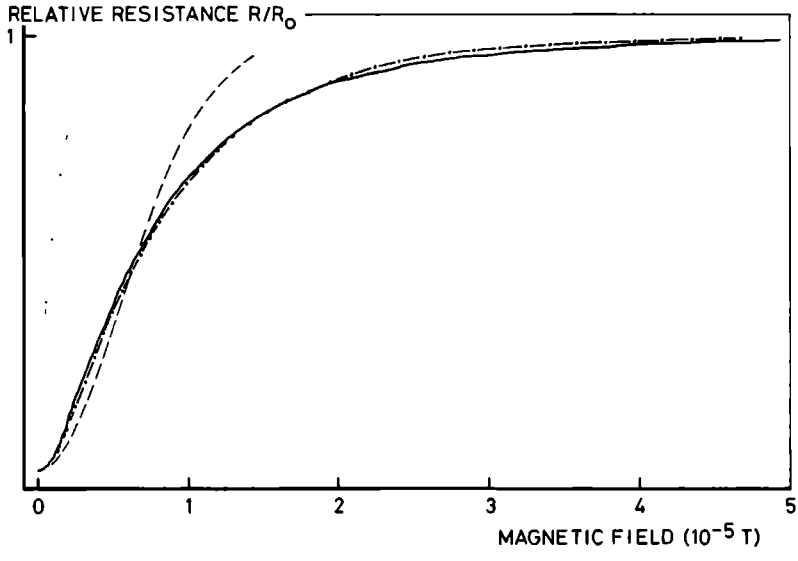

Fig. 4.22 Fit of the AR signal as a function of applied magnetic field. The calculated curves have been normalized to the measured result (solid curve) at B = 0. The dotted curve gives the result in the case of ideal AR, yielding an amplitude about 45 times larger than the measured one. Notice, that the measured curve is much broader than is allowed for ideal AR. The dashed curve results from a Gaussian deviation in the angle of reflection at the N-S interface, the amplitude being still 2.5 times too large. The dot-dashed curve represents the final fit, resulting from an exponential deviation in the angle of reflection [Eq. (4.35)]; an excellent fit can be made for A = 0.71.

exactly. If we assume that there is an uncertainty in the angle of reflection, given by, say, a Gaussian:

$$P(\gamma) \sim \exp[-\gamma^2/\gamma_o^2] \tag{4.34}$$

with γ the deviation from the ideal angle of reflection, the point $\vec{r}(B)$ given by Eq. (4.29) becomes a finite area spot, resulting in a broadening of the signal and a decrease of its amplitude. It is no longer pos-

sible to calculate simply the overlap of two spots; the integrations have to be performed over all angles of incidence and over the point contact area. For $\gamma_0 = 2.1 \cdot 10^{-4}$ rad, the halfwidth of the calculated resistance dip is equal to the halfwidth of the measured signal, shown as the dashed curve in Fig. 4.22. Although the intensity has been reduced, it is still 2.5 times too large; more importantly the line shape is not correct either. However, the measured curve can be fitted surprisingly well if the uncertainty in the reflection is given by

$$P(\gamma) \sim \exp[-\gamma/\gamma_0] \qquad (4.35)$$

Again for $\gamma_0 = 2.1 \cdot 10^{-4}$ rad and A = 0.7 a very good fit is found as can be seen from the dot-dashed curve in Fig. 4.22. The found AR probability, A = 0.7, is in very good agreement with the value for an ideal Ag-Pb interface, equal to 0.7 ± 0.2, as has been noted above.

From the obtained values of γ_0 it is clear that the single point contact technique is a very sensitive method of observing deviations of the electron paths - even at the level of one thousandth of a degree.

The following processes could be responsible for the small amplitudes and the broad signals.

1. The retro-reflection at the N-S interface is not ideal, for example due to defects at the interface.
2. The quasiparticle trajectories in the normal metal deviate from the ideal ones. A possible cause could be the very small angle scattering by the long range strain field of dislocations[23].

These processes give also an explanation for the discrepancies in the results obtained with the double point contact technique.
In the first place, because the focusing spot of Andreev-reflected quasiparticles at the crystal surface has been enlarged, it is clear why the measured AR signals, as a function of the direction of the applied magnetic field with respect to the line connecting the point contacts (Fig. 4.15), were larger than was expected from computer simulations (cf. Fig. 4.9).
In the second place, the apparent dependence of the AR probability, A, on the distance between the point contacts, L, can be an indication that

the broadening, or at least part of it, has been caused by deviations of the quasiparticle trajectories in the normal metal crystal. When L is increased, the path length for EF, l_p^{EF}, increases more than the path length for AR, l_p^{AR}, because l_p^{EF} is directly proportional to L, whereas l_p^{AR} varies only from twice the thickness of the normal metal, 2D, for L = 0 to πD for L = 2D. This means that deviations of the quasiparticle trajectories result in a stronger decrease of the EF signals compared to the AR signals, and so in an apparent L dependence of A.

4.4.3 *Andreev reflection as a function of applied dc voltage*

There remains now only one parameter, namely the barrier strength Z, which appears in the expression for the AR probability A [Eq. (4.2)]. Because A is so drastically dependent on energy (cf. Fig. 4.3), it must be possible to fix Z accurately from measurements of the point contact resistance as a function of the electron energy.

As has been noted before (see Figs. 4.4 and 4.5), on AR the quasiparticle looses some momentum. Because in the measurements of the contact resistance as a function of applied magnetic field the quasiparticle energies were almost zero, the difference in momentum before and after AR was neglected. In the measurements as a function of applied voltage, however, this is no longer correct, as will be shown below. Analogous to specular reflection the momentum component parallel to the N-S interface is conserved, causing a deviation in the angle of reflection. This deviation depends on the angle of incidence and the energy of the quasiparticle. Notice, that the energy is conserved in the AR process (Fig. 4.4), with respect to the Fermi energy. Starting from the boundary conditions for momentum and energy, the deviation between the angle of incidence and reflection, for excitation energies small compared to the Fermi energy, is found to be:

$$\delta\theta = (\varepsilon/\varepsilon_F)\tan\theta \qquad (4.36)$$

with ε the energy of the quasiparticle with respect to the Fermi energy ε_F, and θ the angle of incidence. This indicates that the quasiparti-

cle, even in the absence of an applied field, usually does not return to its starting point at the upper crystal surface, but at a distance $a(\varepsilon,\theta)$, given by

$$a(\varepsilon,\theta) \simeq \frac{D\delta\theta}{\cos^2\theta} = \frac{\varepsilon D \sin\theta}{\varepsilon_F \cos^3\theta} \qquad (4.37)$$

with D the thickness of the normal metal. Also the electron-phonon interaction has to be taken into account. The mean free path is now given by $1/\ell = 1/\ell_{imp} + 1/\ell_{ep}$, where for small energies

$$\frac{1}{\ell_{ep}(\varepsilon)} = \frac{1}{v_F \tau(\varepsilon)} = \frac{2\pi}{v_F \hbar} \int_0^{\varepsilon/\hbar} d\omega\ \alpha^2(\omega)F(\omega) \qquad (4.38)$$

is the energy-dependent phonon-emission length[14] at energy ε. Assuming a quadratic behaviour of $\alpha^2(\omega)F(\omega)$ for Ag at low energies, we find for ℓ_{ep}:

$$\ell_{ep}(\varepsilon) = C/\varepsilon^3 \qquad (4.39)$$

where $C = 4400 \pm 700\ \mu m(meV)^3$, found by fitting Fig. 4.20 on the α^2F function Shalov and Yanson found for Ag[21]. The contact resistance as a function of energy now becomes:

$$\frac{R(\varepsilon)}{R_S} = \left[1 + \frac{b^2 A(\varepsilon)}{\pi D^2 \gamma_o^2} \int_{A_c} d\vec{r} \int_0^1 du \int d\gamma\ a(\varepsilon,u)\ u\ e^{\left(-\gamma/\gamma_o - 2D/\ell u\right)}\right]^{-1} \qquad (4.40)$$

where the first integral runs over the contact area, A_c, and $\cos\theta$ has been replaced by u. The energy dependent AR probability, A, is given by Eq. (4.2). Furthermore, it is assumed that for the energies of interest (<2 meV), apart from AR the contact resistance has an Ohmic behaviour. As all other parameters are known already, the quality of the N-S interface follows directly from Eq. (4.40) fitted to the measured resistance as a function of applied voltage by varying the barrier strength Z in Eq. (4.2). The best fit was found for Z = 0.3, shown in Fig. 4.23 as the dashed curve together with the measured contact resistance as a

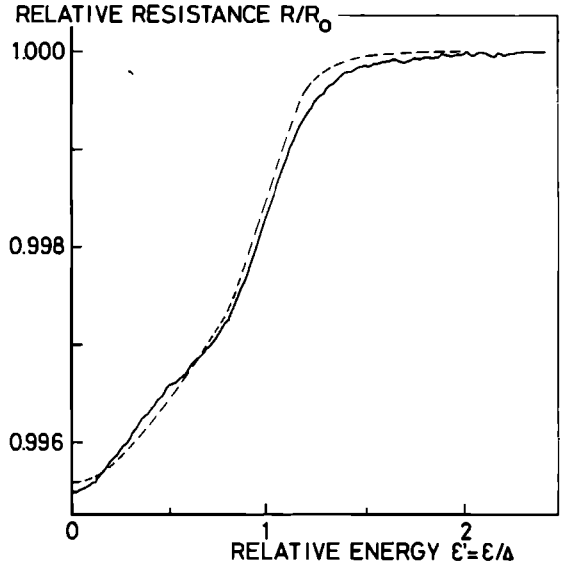

Fig. 4.23 Fit of the measured AR signal (solid curve) as a function of applied dc voltage. The calculated result with Z = 0.3 has been displayed as the dashed curve.

function of applied voltage (solid curve). However, the proportionality constant in the electron-phonon length, ℓ_{ep}, had to be taken 2200 μm(meV)^3. Also the relatively large modulation voltage (0.56 mV peak-to-peak) has been taken into account. The small deviation of the calculated from the measured curve at the gap energy might indicate that the gap energy of superconducting Pb at 1.2 K equals 1.44 meV instead of 1.40 meV, given by Ref. 17.

4.5 *Concluding remarks*

We conclude that we have observed the Andreev reflection process directly by focusing the Andreev-reflected quasiparticles on a point contact. This was performed both with the double point contact technique, where an applied magnetic field was responsible for the focusing

of the quasiparticles, and with the single point contact technique, where in the absence of an external magnetic field focusing could be observed as a function of the quasiparticle energy. In spite of the fact that the signal intensities were very small compared to the simple model for Andreev reflection, we can conclude that there is almost perfect retro-reflection in the Andreev reflection process (within $2 \cdot 10^{-4}$ rad), and that the single point contact technique in particular is very sensitive to deviations of the electron paths - even of the order of 10^{-5} rad. The probability for Andreev reflection, A, at the normal-metal-superconductor interface is found to be 0.7 at zero excitation energy. This is in very good agreement with 0.7 ± 0.2, the value for a perfect Ag-Pb interface.

We are grateful to Ing. T. J. Gortenmulder and late Dr. B. Knook of the Kamerlingh Onnes Laboratory, Leiden, for growing the silver single crystal from the melt, and Ir. L. W. M. Schreurs for orienting and spark-cutting the sample. This work is part of the research program of the Stichting voor Fundamenteel Onderzoek der Materie and was made possible by financial support from the Nederlandse Organisatie voor Zuiver Wetenschappelijk Onderzoek.

References

1. A. F. Andreev, Zh. Eksp. Teor. Fiz. 46, 1823 (1964) [Sov. Phys. -JETP, 19, 1228 (1964)].
2. I. P. Krylov, in Soviet Scientific Review, Section A: Physics Reviews edited by I.M. Khalatnikov, (Harwood Academic Publishers, London, 1980), Vol. 2, p. 85.
3. I. L. Landau, ZhETF Pis. Red. 11, 437 (1970) [JETP Lett. 11, 295 (1970)].
4. I. P. Krylov, and Yu. V. Sharvin, ZhETF Pis. Red. 12, 102 (1970) [JETP Lett. 12, 71 (1970)].
5. W. J. Tomasch, Phys. Rev. Lett., 15, 672 (1965).
6. J. M. Rowell, Phys. Rev. Lett., 30, 167 (1973).
7. G. E. Blonder, and M. Tinkham, Phys. Rev. B 27, 112 (1983).
8. V. S. Tsoi, ZhETF Pis. Red., 19, 114 (1974), [JETP Lett., 19, 70 (1974)].
9. V. S. Tsoi, Zh. Eksp. Teor. Fiz., 68, 1849 (1975), [Sov. Phys.-JETP, 41, 927 (1976)].
10. V. S. Tsoi, J. Bass, P. A. M. Benistant, H. van Kempen, E. L. M. Payens and P. Wyder, J. Phys. F: Metal Phys. 9, L221 (1979).
11. P. A. M. Benistant, H. van Kempen, and P. Wyder, to be published.
12. S. I. Bozhko, V. S. Tsoi and S. E. Yakovlev, Pis'ma Zh. Eksp. Teor. Fiz., 36, 123 (1982), [JETP Lett., 36, 152 (1982)].
13. A Sharvin junction is metallic junction in the extreme Knudsen regime ($\ell/b \gg 1$, with ℓ the electron mean free path and b the contact radius).
    Yu. V. Sharvin, Zh. Eksp. Teor. Fiz. 48, 984 (1965) [Sov. Phys. JETP 21, 655 (1965)].
14. A. G. M. Jansen, A. P. van Gelder, and P. Wyder, J. Phys. C: Solid St. Phys. 13, 6073 (1980).
15. P. G. DeGennes, Superconductivity of Metals and Alloys (Benjamin, New York, 1966), Chap. 5.
16. G. E. Blonder, M. Tinkham and T. M. Klapwijk, Phys. Rev. B, 25, 4515 (1982).

17. W. L. McMillan, and J. M. Rowell in Superconductivity, edited by R. Parks (Marcel Dekker, New York, 1969), Vol 1, p. 561.
18. S. Shih, Z. G. Khim, G. B. Arnold, and W. J. Tomasch, Phys. Rev. B 24, 6440 (1981).
19. Cominco Ltd., Trail, B. C., Canada.
20. A. C. Ehrlich, J. Mat. Science 9, 1064 (1974).
21. Yu. N. Shalov, and I. K. Yanson, Fiz. Nizk. Temp. 3, 99 (1977) [Sov. J. Low Temp. Phys. 3, 48 (1977)].
22. B. Lengeler, W. R. Wampler, R. R. Bourassa, K. Mika, K. Wingerath, and W. Uelhoff, Phys. Ref. B 15, 5493 (1977).
23. Y. K. Chang, and R. J. Higgins, Phys. Rev. B 12, 4261 (1975).

VOLUME 51, NUMBER 9 PHYSICAL REVIEW LETTERS 29 AUGUST 1983

Direct Observation of Andreev Reflection

P. A. M Benistant, H. van Kempen, and P. Wyder
Research Institute for Materials, University of Nijmegen, Toernooiveld, 6525 ED Nijmegen, The Netherlands
(Received 18 January 1983)

An experiment is presented which allows the direct observation of the reflection of conduction electrons in a normal metal at a normal-metal–superconductor interface (Andreev reflection). The experimental findings are in agreement with a change of the quasiparticle-excitation branch on reflection (electron-hole transition) The Andreev-reflection probability can be estimated from the experimental results.

PACS numbers: 74.30.Gn, 73.40.Jn, 74.90.+n

Andreev[1] predicted that at a normal-metal–superconductor interface a conduction electron in the normal metal will be reflected in such a way that it changes into another branch of the quasiparticle excitation spectrum, i.e., the signs of all three velocity components, the sign of the charge, and the sign of the effective mass of the incoming electron are reversed on reflection (electron-hole transition).[2,3] This is contrary to the usual and well-known laws of reflection, where a particle at an interface between two media is reflected in either a specular or diffuse way. Qualitatively, this peculiar and interesting new scattering process can be understood in the following pictorial way If the energy of the incoming electron is smaller than the gap energy of the superconductor and a current passes from the normal metal into the superconductor, the electron has to condense into the ground state of the superconductor as one of the partners of a Cooper pair. This condensation process requires another electron from the normal metal as the second partner of the Cooper pair, leading to an extra current into the superconductor known as "excess current".[3] Therefore, in the normal metal an electron is missing, which can be interpreted as the reflection of a hole with opposite velocity, mass, and charge, properly taking into account the conservation of momentum, mass, and charge of the total system. The occurrence of this so called Andreev reflection (AR) has previously been shown, e.g., by tunneling experiments,[4,5] where the change in the tunneling density of states due to the quantum mechanical interference effects of these different states is measured, or by Gantmakher-resonance experiments in the intermediate state.[2] In this paper, we present direct ballistic observations of the peculiar AR way in which electrons can be reflected at an interface.

To observe the reflection at the normal-metal–superconductor interface we use a double-point-contact electron-focusing technique. It has been demonstrated before[6-8] that with this technique information can be achieved about the orbits of the charge carriers within a metal single crystal and their reflection from its surface. Basically this technique consists of placing two point contacts on a flat surface of a metal single crystal. Electrons are injected into the crystal at one point contact (the emitter) and are bent around by a homogeneous magnetic field, parallel to the surface and perpendicular to the line connecting the point contacts. Either directly or via reflections (e.g., at boundaries) they reach the other point contact (the collector). The electrons follow orbits lying on the Fermi surface in a plane perpendicular to the applied field. Depending on the topology of the Fermi surface, one can have closed orbits surrounding states with lower energy ("electron" orbits) or higher energy ("hole" orbits). It should be emphasized here that these sorts of "holes" are entirely different from the "missing electron" type of holes described above. Electrons on "electron" orbits are bent around by the field in the same direction as free electrons, electrons on "hole" orbits, however, are bent in the opposite direction. Note that the charge of the electrons on both kinds of orbits is the same. At the collector a field-dependent voltage is measured. If the magnetic field strength is such that exactly those electrons injected at the emitter normally to the crystal surface reach the collector, there is an accumulation of electrons at the collector and therefore a voltage peak [electron focusing (EF)[6]].

In the experiment described in this paper the emitter and collector are placed on a thin silver single crystal with a thickness comparable with the mean free path of the charge carriers. At sufficiently low magnetic field strengths, the electrons injected into the crystal at the emitter

can reach the other side of the crystal where a Pb layer has been deposited. On specular reflection only the velocity component perpendicular to the interface changes sign, on AR, however, all velocity components change sign. As both charge and mass have been reversed for the AR particles, in magnetic fields they follow the same trajectories as the original particles. This is illustrated in Fig. 1. With the help of the quasiclassical laws of the dynamics of conduction electrons in metals,[9] using the proper parameters for the Fermi surface of Ag,[10] trajectories are drawn for different angles of emission. Circular orbits, as a good approximation to the electrons moving over the "electron" (belly) orbits of the Ag Fermi surface, are shown in Figs. 1(a) and 1(b). As can be seen from the figure, only those particles that are reflected in Andreev fashion at the Ag-Pb interface have an accumulation point at the upper Ag surface and therefore can be focused on the collector, provided the magnetic field has the correct orientation and strength. Figure 1(c) summarizes the kind of signals that can be expected due to EF in this type of experiment: electrons moving over "electron" orbits (belly), observed directly (α_1) or via reflection at the top surface (α_2); electrons moving over "hole" orbits (four-cornered rosette) (β_1, β_2), and AR particles with a hole ("missing electron") character moving over belly orbits (γ). Figure 1(d) shows the orbits α and β on the Ag Fermi surface in the extended-zone scheme.

The samples are slices, spark cut from a single crystal of 99.9999+% purity.[11] We report on two crystals one with its surface perpendicular to the [01$\bar{1}$] direction (sample 1) and one with its surface perpendicular to the [001] direction (sample 2). After spark cutting, the samples were polished by mechanical and chemical techniques, to thicknesses of about 0.23 and 0.21 mm, respectively. Then they were annealed at 600 C in vacuum in order to release mechanical stresses. Before the deposition of the Pb layer the samples were sputter cleaned in a glow discharge of N_2 for about 20 min at a pressure of 10^{-1} Torr. Finally, a layer of about 1.5 μm Pb was evaporated at a pressure of 10^{-4} Torr for sample 1, and of 10^{-6} Torr for sample 2, at a temperature of about 50 °C. Parts of the samples were kept free of Pb for measurements with and without a normal-metal–superconductor interface using the same sample.

The two point contacts were made of 96 μm-diam tungsten wires, with sharp points of about 1 μm diam etched electrolytically in 1N KOH [8] The measurements were performed at tempera-

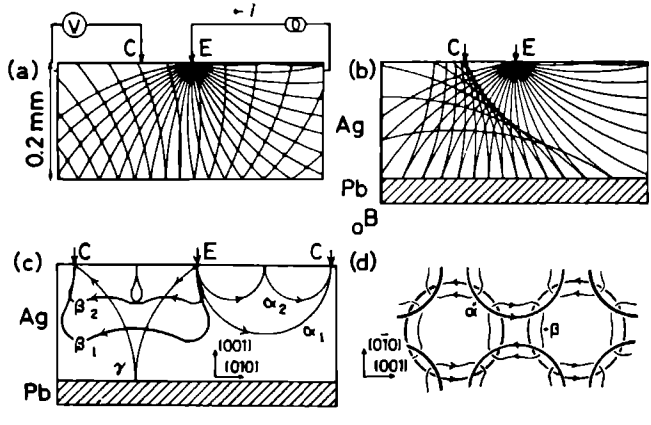

FIG. 1. Trajectories for electron focusing in Ag crystal (a) Orbits of free electrons in a metal in a homogeneous magnetic field with specular reflection at the bottom of the metal; (b) the same orbits but now in the case of Andreev reflection at the bottom of the metal [(a) and (b) are drawn to scale, using a sample thickness D = 0 2 mm, a Fermi velocity of Ag v_F = 1 38×10^8 cm/s, and a magnetic field B = 0 017 T]; (c) different types of orbits at the focusing field strengths in a silver single crystal (see text) (α_1, α_2) "electron" (belly) orbits, (β_1,β_2) "hole" (four-cornered rosette) orbit, (γ) Andreev-reflected particle on belly orbits; (d) closed orbits on the Ag Fermi surface in the extended-zone scheme perpendicular to the [100] axis showing a belly (α) and the four-cornered-rosette orbit (β)

tures between 1 and 4 K, i.e., far below the critical temperature for superconductivity of Pb.

Reproducible results were obtained for many different positions of the point contacts on the crystals. Some typical magnetic field sweeps are shown in Fig. 2. For sample 1 [Figs. 2(a) and 2(b)] the magnetic field has been directed along the [111] axis and for sample 2 [Fig. 2(c)] along the [100] axis. The focusing of "electron" (belly) orbits (α_1) can be seen, as well as the reflected electrons (α_2, α_3), also the "hole" (four-cornered rosette) orbits can be seen in Fig. 2(c) (β_1, β_2). AR is displayed in Figs. 2(b) and 2(c) (γ). The ratio of the first and second peaks (the signals at α_1 and α_2, or respectively, β_1 and β_2) gives the reflection coefficient for the given Ag surface[8] ($\simeq$0.3 for sample 1 and $\simeq$0.7 for sample 2). That the signals indicated by γ are indeed due to AR is supported by the following experimental observations: the absence of the signal when no Pb is present [Fig. 2(a)], the sign of the signal, and the sign and strength of the focusing magnetic field. The construction displayed in Fig. 1(a) shows that in the absence of the Pb layer no focusing can take place at the collector of electrons reflected specularly at the bottom of the sample. As Figs. 2(b) and 2(c) show, the signals γ have a sign opposite to the sign of the signals α and β, this is in agreement with AR where the sign of the charge of the particles is inverted on reflection. Figure 1(c) shows that the orientation of the magnetic field on focusing of AR particles is opposite to the case of EF, again in agreement with our measurements [Figs. 2(b) and 2(c)]. It can be shown by straightforward geometrical arguments that the relation between the focusing magnetic field strength B_0 and the point-contact distance L is given by

$$B_0 = A/L \qquad (1)$$

with $A = 2\hbar k_F/e$, k_F the radius of the free-electron Fermi sphere. For the circular belly orbits in Ag one finds $A = 1.58\times10^{-2}$ mm T.[10] Similarly one can deduce a relation between L, the thickness D of the normal metal, and the focusing field B_0^{AR} in the case of AR

$$B_0^{AR} = -2AL/(L^2+4D^2) \quad (L \lesssim 2D). \qquad (2)$$

From Eqs. (1) and (2) there follows a relation between the focusing fields

$$B_0^{AR} = -2B_0/[1+(2DB_0/A)^2]. \qquad (3)$$

Experiments with many different point-contact distances confirmed Eq. (3), except that for sample 1 a thickness had to be assumed which is 25% larger than the measured thickness. This deviation is larger than the estimated error in D of 5% and is not yet understood. For sample 2 the agreement is within the thickness variation of 15% over the sample.

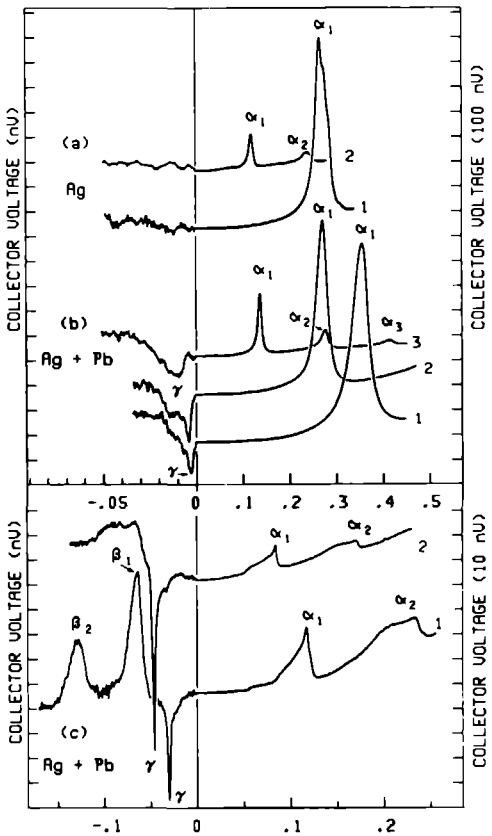

FIG. 2. Electron focusing in Ag single crystal. Experimental results for sample 1 [(a) without and (b) with a Pb layer on the bottom surface] and for sample 2 (c), showing the focusing of electrons and holes on different types of orbits: (α) "electron" (belly) orbits, focused directly (α_1) or via one or more reflections from the upper Ag surface (α_2, α_3); (β_1, β_2) "hole" (four-cornered rosette) orbit; (γ) Andreev-reflected particles on belly orbits. Increasing numbers labeling curves in each part stand for increasing point-contact distances, the different distances lead to different values of the resonant fields. Note the different voltage and field scales used for the positive and negative magnetic field orientations.

The size of the Andreev signal gives a measure of the probability for AR at the Ag-Pb interface.[3] Taking into account only the electrons emitted in the plane through the emitter and collector contacts perpendicular to the magnetic field and estimating the mean free path ($l \gtrsim 0.2$ mm) from the point-contact distance dependence of the electron-focusing signal, we find for sample 1 a probability for AR of about 1/250. This has to be considered as an upper limit because in the case of AR electrons that are emitted in directions outside the above mentioned plane can also be focused on the collector. (A detailed discussion of the three-dimensional problem will be given elsewhere.) The small probability indicates a strong disturbance of the Ag-Pb interface, e.g., by a large oxide barrier. This has probably been caused by our sample preparation technique, where we prepared the Ag surface outside the evaporator system. In sample 2 the AR probability is considerably larger (≈ 0.5), probably because of a more careful fabrication of the interface (e.g., evaporation at 10^{-6} Torr instead of 10^{-4} Torr).

We conclude that we have observed the Andreev reflection of electrons directly. The expected reversal of the signs of the charge, the mass, and the quasiparticle excitation velocity components on Andreev reflection at a normal-metal–superconductor interface is confirmed. This experiment is an application of the double-point-contact technique, which seems to be a promising method to study surfaces by electron reflection from the inside of a metal single crystal.

The authors wish to thank Dr. B. Knook and Ing. T. J. Gortenmulder of the Kamerlingh Onnes Laboratory, Leiden, for growing the silver single crystal from the melt and Ir. L. W. M. Schreurs for orienting and spark cutting the samples. This work is part of the research program of the Stichting voor Fundamental Onderzoek der Materie and was made possible by financial support from the Nederlandse Organisatie voor Zuiver-Wetenschappelijk Onderzoek.

Note added.—Very recently another transverse electron-focusing experiment has been reported which, though using a different geometry, also allows the observation of AR.[12] We thank Professor V. S. Tsoi for bringing his beautiful work to our attention.

[1]A. F. Andreev, Zh. Eksp. Teor. Fiz. 46, 1823 (1964) [Sov. Phys. JETP 19, 1228 (1964)].

[2]I. P. Krylov, in *Soviet Scientific Reviews, Section A Physics Reviews*, edited by I. M. Khalatnikov (Harwood Academic Publishers, London, 1980), Vol. 2, p. 85.

[3]G. E. Blonder, M. Tinkham, and T. M. Klapwijk, Phys. Rev. B 25, 4515 (1982).

[4]W. J. Tomasch, Phys. Rev. Lett. 15, 672 (1965).

[5]J. M. Rowell, Phys. Rev. Lett. 30, 167 (1973).

[6]V. S. Tsoi, Pis'ma Zh. Eksp. Teor. Fiz. 19, 114 (1974) [JETP Lett. 19, 70 (1974)].

[7]V. S. Tsoi, Zh. Eksp. Teor. Fiz. 68, 1849 (1975) [Sov. Phys. JETP 41, 927 (1976)].

[8]V. S. Tsoi, J. Bass, P. A. M. Benistant, H. van Kempen, E. L. M. Payens, and P. Wyder, J. Phys. F 9, L221 (1979).

[9]See, e.g., C. Kittel, *Quantum Theory of Solids* (Wiley, New York, 1963), Chap. 11.

[10]See, e.g., C. Kittel, *Introduction to Solid State Physics* (Wiley, New York, 1967), Chaps. 7 and 9.

[11]Cominco Ltd., Trail, B. C., Canada.

[12]S. I. Bozhko, V. S. Tsoi, and S. E. Yakovlev, Pis'ma Zh. Eksp. Teor. Fiz. 36, 123 (1982) [JETP Lett. 36, 152 (1982)].

This thesis deals with an experimental investigation of the focusing of electrons in pure metal single crystals by means of a uniform magnetic field. Two point contacts are made on the surface of a metal single crystal. Through one point contact (the emitter) electrons are injected into the crystal, and at the other point contact (the collector) the voltage is measured as a function of applied magnetic field. Due to this magnetic field, directed parallel to the crystal surface and perpendicular to the (imaginary) line connecting the point contacts, the electrons are deflected, and they will reach the crystal surface again. A maximum in the collector voltage is measured if the strength of the magnetic field is such that electrons injected into the crystal at the emitter perpendicular to the surface, reach the collector. Also at magnetic field strengths that are 2, 3, or more times this value, voltage peaks can be measured at the collector. These are caused by focusing of electrons reflected specularly from the crystal surface between the point contacts 1, 2, or more times. The ratio between the different voltage peaks gives directly the coefficient for specular reflection for the given crystal surface.

After a general introduction, chapter II gives a review of the experimental technique together with theoretical background based on semiclassical theory, which is adequate for this technique. Experimentally obtained results from a pure silver single crystal are presented and compared with calculations based on the theory. Although the crystal surface looked rather rough under a microscope, the measured coefficients for specular reflection are so large, that the surface must be flat on an atomic scale. In an applied magnetic field the electrons traverse orbits in wave vector space, that are intersections of the metal Fermi surface with planes perpendicular to the direction of the field. Extremes in the diameters of particular orbits on the Fermi surface have been measured and compared to a spherical (free electron approximation) Fermi surface for silver. Our results, in agreement with other experiments, indicate that apart from the <111> directions the Ag Fermi surface does approximate closely to a sphere. However, the measured variety in intensity and form of the collector voltage for orbits

on different parts of the Ag Fermi surface, show that with this technique very small variations in the shape of the Fermi surface can be measured.

Chapter III describes an application of the technique to an aluminium single crystal. Here also the influence of the shape of the Fermi surface on the signal form as well as on the strength of the focusing magnetic field can be seen clearly. A temperature and magnetic field dependent disturbance of the collector voltage was measured, probably due to superconducting regions under the collector. These could have been formed by chemical contaminations or crystal deformations below the point contacts, due to the spot-welding of the tungsten point contacts to the crystal surface.

The last two chapters deal with the peculiar way an electron in a normal metal reflects from a normal-metal-superconductor interface. This, so called Andreev reflection, occurs because an electron in a normal metal with an energy smaller than the gap energy of the superconductor, cannot enter the superconductor as a quasiparticle. Instead, it reflects as a hole with a sign reversal of charge, mass, and velocity, contrary to specular reflection where the mass and charge are conserved and only the velocity component perpendicular to the surface is reversed. Andreev reflection has been observed using the double point contact technique, but also using the single point contact technique, where the voltage is measured across the emitter contact. The point contacts were placed on one side of a thin silver single crystal slab, with a superconductor (Pb) deposited on the other side. Because the electron mean free path in the slab was much larger than the slab thickness, the injected electrons could reach the interface without scattering. The configuration was such that only the Andreev-reflected holes could be focused on the collector or emitter respectively, depending on the strength of the applied magnetic field. In particular the single point contact technique is extremely sensitive to deviations of the electron paths - even in the order of one thousandth of a degree.

Dit proefschrift behandelt experimenteel onderzoek van het focusseren van electronen in zuivere éénkristallijne metalen door middel van een homogeen magneetveld. Door een puntcontact (de emitter) worden electronen in het metaal geïnjecteerd, terwijl over een tweede puntcontact (de collector), op een bepaald punt van het metaal-oppervlak, de spanning wordt gemeten als functie van het aangelegde magneetveld. Onder invloed van dit magneetveld, dat evenwijdig aan het oppervlak en loodrecht op de (denkbeeldige) lijn tussen de puntcontacten gericht is, zullen de geïnjecteerde electronen worden afgebogen en weer bij het oppervlak terecht komen. Er wordt een maximum in de spanning over de collector gemeten, indien de veldsterkte zodanig is, dat electronen die loodrecht op het metaal-oppervlak worden geïnjecteerd, precies bij de collector terechtkomen. Ook bij veldsterkten die 2, 3 of meer maal zo groot zijn als bovengenoemde veldsterkte, kunnen er maxima in de spanning worden gemeten, door het focusseren van electronen die 1, 2 of meer maal spiegelend tegen het oppervlak zijn gereflecteerd alvorens de collector te bereiken. De verhouding tussen de verschillende maxima geeft direct de coëfficiënt voor spiegelende reflectie van het betreffende metaal-oppervlak.

Na een algemene inleiding geeft hoofdstuk II een overzicht van de experimentele techniek en een theoretische achtergrond gebaseerd op de semi-klassieke theorie, die toereikend is voor deze techniek. De experimentele resultaten gemeten aan een zuiver zilveren éénkristal worden gepresenteerd en vergeleken met berekeningen die gebaseerd zijn op de theorie. Alhoewel het kristal-oppervlak er tamelijk ruw uitzag onder een microscoop, zijn de gemeten coëfficiënten voor spiegelende reflectie zo groot, dat het oppervlak glad moet zijn op atomaire schaal. Vanwege het magneetveld doorlopen de electronen banen die identiek zijn aan doorsnijdingen van het Fermi-oppervlak loodrecht op de richting van het aangelegde veld. Extrema in de diameters van bepaalde, niet noodzakelijk extremale, banen op het Fermi-oppervlak zijn gemeten en vergeleken met een bolvormig Fermi-oppervlak voor zilver (vrije electron benadering). Het blijkt dat, buiten de <111> richtingen, het Fermi-oppervlak van zilver inderdaad bijna bolvormig is, in overeenstemming met andere experimenten. De gemeten verscheidenheid in de intensiteit

en vorm van de collectorspanning voor banen op verschillende gedeelten van het Fermi oppervlak van zilver tonen echter aan, dat met deze techniek zelfs zeer kleine vervormingen van het Fermi-oppervlak gemeten kunnen worden.

Hoofdstuk III laat een toepassing van deze techniek zien op éénkristallijn aluminium. Ook hier is de invloed van de vorm van het Fermi-oppervlak zowel op de signaalvorm als op de sterkte van het focusserende magneetveld duidelijk te zien. Er werd een temperatuur en magneetveld afhankelijke storing in de collectorspanning gemeten, veroorzaakt door het normaal worden van supergeleidende gebieden in het metaal onder de collector. Deze zouden kunnen ontstaan door chemische verontreinigingen in het kristal of vervormingen van het kristalrooster onder de puntcontacten tengevolge van het vastlassen van de wolfraam puntcontacten op het kristaloppervlak.

De laatste twee hoofdstukken behandelen de merkwaardige manier waarop een electron in een normaal metaal reflecteert aan een normaal-metaal-supergeleider overgang. Deze zogenaamde Andreev-reflectie treedt op, omdat een electron in het normale metaal, met een energie kleiner dan de gap-energie van de supergeleider, deze supergeleider niet als quasideeltje kan binnengaan. Het wordt daarentegen als gat gereflecteerd met massa, lading en snelheid tegengesteld aan de massa, lading en snelheid van het inkomende electron. Dit in tegenstelling tot spiegelende reflectie, waarbij massa en lading behouden blijven en alleen het teken van de snelheidscomponent loodrecht op het oppervlak omkeert. Andreev-reflectie is zowel met de dubbel puntcontacttechniek waargenomen als met de enkel puntcontacttechniek, waarbij over de emitter ook de spanning wordt gemeten. De puntcontacten werden op één zijde van een dun zilveren éénkristal geplaatst, terwijl de supergeleider (lood) op de andere zijde was aangebracht. Omdat de gemiddelde vrije weglengte van de electronen veel groter was dan de dikte van het kristal, konden de geïnjecteerde electronen zonder botsingen de supergeleider bereiken. De configuratie was zodanig, dat alleen Andreev-gereflecteerde gaten gefocusseerd konden worden respectievelijk op de collector of de emitter, afhankelijk van de sterkte van het aangelegde magneetveld. Het blijkt dat met deze techniek nog afwijkingen van de electronbanen waargenomen kunnen worden in de orde van een duizendste graad.

CURRICULUM VITAE

P.A.M. Benistant

Geboren : 4 mei 1955 te Amsterdam.

1967 - 1973 : Gymnasium B, Thomas à Kempis College, Arnhem.

1973 : Begin studie Natuurkunde, K.U. Nijmegen.

sept. 1980 : Doctoraalexamen Experimentele Natuurkunde, hoofdvak Vaste Stoffysica.

1980 - 1984 : Promotieonderzoek op de afdeling Experimentele Natuurkunde 4, Faculteit der Wiskunde en Natuurwetenschappen, Katholieke Universiteit Nijmegen, in het kader van een FOM-beleidsruimte projekt onder leiding van Prof. P. Wyder.

Stellingen

I

De toepassing van supergeleidende magneten bij High Gradient Magnetic Separation wordt eerder gerechtvaardigd door de aan hogere magneetvelden gerelateerde grotere verwerkingscapaciteit dan door de eveneens optredende verbetering in de separatie-efficientie.

II

Als gevolg van het additionele karakter van de magnetische wisselwerking tussen gedispergeerde deeltjes kan magnetische flocculatie worden toegepast ter bepaling van de colloïdchemische eigenschappen van deze deeltjes.

R. P. A. R. van Kleef, H. W. Myron, and P. Wyder, J. Appl. Phys. 54, 4223 (1983).

III

De experimenten van Gubankov en Margolin aan de stroom - spanningskarakteristiek van supergeleider - normaal metaal puntcontacten onder invloed van microgolfstraling vormen geen ondersteuning van het AVZ-model (Artemenko, Volkov, en Zaitsev). In het microgolf gebied levert klassieke gelijkrichting nog dezelfde resultaten.

V. N. Gubankov and N. M. Margolin, Zh. Eksp. Teor. Fiz. 80, 1419 (1981) [Sov. Phys. JETP 53, 727 (1981)];

C. A. Hamilton and S. Shapiro, Phys. Rev. B 2, 4494 (1970).

IV

Bij het opstellen van een dispersievergelijking voor lopende electromagnetische golven in een tunneljunctie moeten de Ohmse verliezen ten gevolge van de geïnduceerde tunnelstroom (Photon Assisted Tunneling) expliciet worden meegenomen.

L. E. Hasselberg, J. Phys. F: Metal Phys. 4, 154 (1974).

V

Van de verschillende mechanismen voor gestimuleerde supergeleiding leent tunnelinjectie zich het best voor een kwantitatieve toetsing van de theorie. Bij tunnelinjectie kan stimulering namelijk beter van opwarming onderscheiden worden dan bij gebruik van bijvoorbeeld microgolven of fononen.

VI

Bij een reactieve botsing tussen een molecuul CF_3X (met X een halogeen zwaarder dan F) en een atoom M (met M een (aard)alkali of zuurstof) kan behalve MX, zoals tot nu toe werd aangenomen, ook MF gevormd worden.

J. C. Whitehead, in Comprehensive Chemical Kinetics, edited by C. H. Bamford and C. F. H. Tipper (Elsevier, Amsterdam, 1982), Vol. 24, Chap. 5, p. 357;

R. J. Buss, S. J. Sibener, and Y. T. Lee, J. Phys. Chem. 87, 4840 (1983).

VII

De mogelijkheid om met de Vacuum Tunneling Microscope electrische circuits op sub-sub-micronschaal te schrijven en te testen is een serieuze poging tot onderzoek waard.

VIII

Het verdient aanbeveling om in studies naar de invloed van hoge magneetvelden op biologische systemen ook de invloed van deze velden op de desorptie en absorptie processen van zuurstof in deze systemen in beschouwing te nemen.

IX

Sollicitanten kunnen de kans een baan te vinden aanzienlijk vergroten door bij hun sollicitatiebrief in plaats van een pasfoto een videoband mee te sturen.

X

De computers die de verkeerslichten op kruispunten sturen, lijken eerder geprogrammeerd om de kruising verkeersvrij te houden dan om voor een vlotte doorstroming van het verkeer te zorgen.

P.A.M. Benistant

Nijmegen, 3 oktober 1984.